

Risk assessment of COVID infection by respiratory droplets from cough for various ventilation scenarios inside an elevator: An OpenFOAM-based computational fluid dynamics analysis

Cite as: Phys. Fluids **34**, 013318 (2022); doi: 10.1063/5.0073694

Submitted: 2 October 2021 · Accepted: 30 December 2021 ·

Published Online: 24 January 2022





View Online



Export Citation



CrossMark

Riddhideep Biswas,¹ Anish Pal,¹ Ritam Pal,² Sourav Sarkar,^{1,a)}  and Achintya Mukhopadhyay¹ 

AFFILIATIONS

¹Department of Mechanical Engineering, Jadavpur University, Kolkata-700032, India

²Department of Mechanical Engineering, The Pennsylvania State University, University Park, Pennsylvania 16802, USA

Note: This paper is part of the special topic, Flow and the Virus.

^{a)} Author to whom correspondence should be addressed: souravsarkar.mech@jadavpuruniversity.in

ABSTRACT

Respiratory droplets—which may contain disease spreading virus—exhaled during speaking, coughing, or sneezing are one of the significant causes for the spread of the ongoing COVID-19 pandemic. The droplet dispersion depends on the surrounding air velocity, ambient temperature, and relative humidity. In a confined space like an elevator, the risk of transmission becomes higher when there is an infected person inside the elevator with other individuals. In this work, a numerical investigation is carried out in a three-dimensional domain resembling an elevator using OpenFoam. Three different modes of air ventilation, viz., quiescent, axial exhaust draft, and exhaust fan, have been considered to investigate the effect of ventilation on droplet transmission for two different climatic conditions (30 °C, 50% relative humidity and 10 °C, 90% relative humidity). The risk assessment is quantified using a risk factor based on the time-averaged droplet count present near the passenger's hand to head region (risky height zone). The risk factor drops from 40% in a quiescent scenario to 0% in an exhaust fan ventilation condition in a hot dry environment. In general, cold humid conditions are safer than hot dry conditions as the droplets settle down quickly below the risky height zone owing to their larger masses maintained by negligible evaporation. However, an exhaust fan renders the domain in a hot dry ambience completely safe (risk factor, 0%) in 5.5 s whereas it takes 7.48 s for a cold humid ambience.

Published under an exclusive license by AIP Publishing. <https://doi.org/10.1063/5.0073694>

I. INTRODUCTION

The ongoing pandemic of COVID-19 has caused an immense loss of lives as well as shattered the global economy, the entire world still suffering from its excruciating shackles. The transmission of SARS-CoV-2 has been responsible for this pandemic and it has been established that the virus spreads through respiratory droplets.^{1–3} Respiratory droplets are exhaled from the mouth or nose during speaking, coughing, or sneezing. The conditions of speaking, coughing, or sneezing can be differentiated with the help of droplet size and velocity spectra and the exhalation velocity of jet from the mouth.^{4,5} The respiratory droplets expelled from the mouth by coughing or sneezing are polydisperse in nature. Kwon *et al.* performed experiments involving particle image velocimetry to study the initial velocity distributions from coughing and sneezing.⁶ Johnson *et al.* performed experiments with an Aerodynamic Particle Sizer in order to obtain the

aerosol size distribution during coughing.⁷ Li *et al.* computationally modeled the evaporation of cough droplets employing the multi-component Eulerian–Lagrangian approach in an inhomogeneous humidity condition.⁸ It is expected that the droplets will follow a projectile motion and eventually settle on the ground. However, during coughing, a turbulent jet is generated by the air puff, which takes the responsibility of carrying the droplets an appreciable amount of distance. While traveling the distance, the droplet undergoes evaporation, which reduces the size of the droplets, thereby helping them to cover more distance. Redrow *et al.* modeled the evaporation and dispersion of cough jet droplets considering sputum for the first time and showed that the human cough includes a turbulent air puff.⁹ Wei *et al.* showed that the droplet spread gets enhanced by the presence of a turbulent air jet.¹⁰ Pal *et al.* investigated the influence of ambient conditions on droplet transport in indoor environments. The droplet trajectories

were calculated considering a turbulent round jet model.¹¹ Chong *et al.* quantified the lifetime of respiratory droplets under different ambient humidity conditions using direct numerical solution (DNS). They have reported that the droplet lifetime can extend even up to 150 times at very high relative humidity (90%).¹² The droplet size can increase initially in cold environments due to the supersaturation of vapor turbulent puff.¹³ Wang *et al.* performed flow visualization and particle image velocimetry to understand the motion of these droplets and utilized those results to establish a physical model for investigating the trajectories of droplets expelled by cough.¹⁴ Pendar *et al.* conducted a wide range study of the velocity distribution, expelled angle, and the size of droplets released from the mouth in order to determine the correct social distance guidelines for different conditions.¹⁵ Dbouk and Drikakis have conducted a computational study to investigate the transport, dispersion, and evaporation of respiratory droplets produced from human cough.¹⁶ If a person is present in an open area like a school ground or market place, the risk of disease transmission depends on the wind velocity due to the available space between two persons. Feng *et al.* carried out a numerical study to investigate the effects of wind and relative humidity on the transportation of respiratory droplets in an outdoor environment for different wind velocity ranges from 0 to 16 km/h.¹⁷ They have found that droplet clouds can travel up to 8 m in the presence of wind. Li *et al.* performed a numerical study on the dispersion of cough droplets with nonvolatile components in a tropical outdoor environment and the dispersion was influenced by the relative humidity and wind speed.¹⁸

In an open space, it has been observed from the above literatures that the wind speed affects the spread of these droplets but the situation becomes alarming in a confined space where the environment is enclosed and if a person coughs, the droplets will remain inside the space for an appreciable amount of time. In recent times, several studies have been performed on aerosol and droplet transmission in different confined spaces like classrooms,¹⁹ aircraft cabins,^{20,21} restaurants,^{22,23} buses,²⁴ and clinics.²⁵ Liu *et al.* performed a laboratory study to investigate the expiratory airflow and particle dispersion in a stratified indoor environment.²⁶ Cheng *et al.* investigated the trajectories of large respiratory droplets in indoor environments under different relative humidity.²⁷ They reported that droplets produced from coughing can travel distances of 1.09 m and that of sneezing can cover a distance of 2.76 m. Yang *et al.* carried out a computational study to capture the dispersion of pathogen-laden respiratory droplets in an enclosed environment like crowded buses.²⁴ Foster *et al.* studied the infection probability in the classroom scenario with masked habitans and different ventilation conditions.¹⁹ Yan *et al.* employed the Lagrangian-based Wells–Riley approach to assess the risk of airborne disease infection in an airliner cabin.²¹ Yan *et al.* numerically investigated the thermal effects of human body on the evaporation and dispersion of cough droplets in an enclosed environment.²⁸ Sen performed a numerical study to investigate the evaporation and transmission of cough droplets in a confined space, like elevator, considering different scenarios by varying, for example, the air ventilation systems, number of persons inside the elevator, direction of ejection, relative humidity, and temperature.²⁹ Dbouk *et al.* showed how modifications in ventilation systems in confined spaces can influence the transmission of airborne virus.³⁰ Agrawal *et al.* have worked on the reduction of the risk associated with cough clouds in a closed space by

modifying the ventilation systems.³¹ It was found that the infected air volume is 23 times the ejected volume of air by cough.

All these works have paid attention to ventilation systems but none of them have studied the risk to which another person will be exposed when he or she tries to board the elevator after the door opens. Respiratory droplets are laden with salt and proteins containing virions. Moreover, in most of these works, pure water droplets have been considered, which does not resemble a real scenario where the droplets are pathogen laden. The droplets contain nonvolatile salts in some specific proportions and these salts contain pathogens. A salt-laden droplet will have thermophysical properties different from that of a pure water droplet, and the thermophysical properties will constantly change with evaporation, unlike pure water. This difference and constant change in thermophysical properties will cause a difference in the mass transfer number and, hence, the evaporation rate, ultimately manifesting itself in a difference in the overall droplet dispersion and trajectory than that of pure water. So, in order to mitigate the above stated problem and to make the simulations and their corresponding results more realistic, our work has implemented this salt model of droplet along with droplet evaporation. In addition, a systematic comparison of the risk of infection from different designs of ventilation along with the safety measures to be adopted in each of the designs has been carried out in this work.

In confined spaces, ventilation plays a significant role, which has been highlighted in the existing literature. When the droplets are inside an enclosed space, they will undergo evaporation, which will transform them into aerosol, and they can remain suspended in the air for longer periods of time. Several works have been reported recently where the aerosol route of virus transmission has been supported with enough evidences.^{16,32–35} The aerosol size is generally considered less than 10 μm , which helps them to remain suspended in the air for longer periods of time. Furthermore, from the recent works, it can be concluded that aerosols constitute the virions that are responsible for the disease transmission.³⁶ So, when a person coughs or sneezes in a confined space like an elevator, the aerosol will remain in the space until it is forced out or it gets any opening to discharge outside. This implies that when an elevator door will open for the passenger who is waiting outside, the passenger will be exposed to a high-risk situation in the elevator if the former passenger inside the lift has just coughed before opening of the door. Face masks may work as a protective gear up to a certain extent but there are limitations. Akhtar *et al.* performed droplet flow visualization experiments to test the effectiveness of five different masks and it was found that except for the N-95 masks, all the other masks showed some amount of droplet leakage.³⁷ Dbouk *et al.* have also worked on the effectiveness of masks to reduce the droplet transmission.³³ The risk assessment of such situations is necessary as it will help to understand the safe time interval between stopping of the elevator and boarding it. Moreover, the assessment can also give information regarding the safe distance that must be maintained from the infected passenger inside the elevator.

In this work, a three-dimensional simulation has been performed to study droplet transmission inside an elevator. An infected passenger is present inside that elevator without a face mask and the passenger is coughing. Different ventilation conditions of the ambience have been investigated by considering both quiescent environments and forced circulation of air in the domain. The dispersion and evaporation of the droplets (including nonvolatile components) have been investigated in

each of the cases. The situation is such that a person has boarded the elevator and before alighting from the elevator, the person coughs. The beleaguered person waiting outside to board the elevator will be oblivious to the threat that looms inside the elevator. Our paper focuses on the risk assessment of this situation for various ventilation conditions along with suggestions of safety measures.

II. PROBLEM FORMULATION

A. Geometry

The computational domain consists of an elevator having a capacity of five persons, which is portrayed in Fig. 1(a), describing its details. The dimension of the elevator is $1.2 \times 1.2 \times 2$ m, which represents a characteristic size of elevators present in housing complexes or small enterprises. The investigation of an elevator of relatively small size is incumbent as the risk associated with a smaller confined space is higher. At the top of the elevator, a circular mounting of 0.6 m

diameter is provided. This top circular mounting is subjected to conditions specific to each scenario, as illustrated further in the Initial and Boundary Conditions section as well as in Table I. This top mounting is a very important part as by altering the boundary conditions on this mounting, the various ventilation situations inside the elevator are realized. In the present study, boundary conditions representing an axial exhaust jet or an exhaust fan at the top opening have been presented. The ventilation slots, 3% of the platform area, have been provided at the lower portion of the elevator side walls (complying with the European EN-81-1 code³⁸). Instead of incorporating a human manikin, the features of the passenger, namely, the head, face, mouth, and remaining body parts, have been represented with rectangular boxes, whose dimensions conform to that of an actual human being in an upright standing position, to reduce the complexity and the computational cost and time. Moreover, since our area of focus in the domain is far away from the passenger, the implementation of a geometry that corresponds to an actual human being will have no effect on

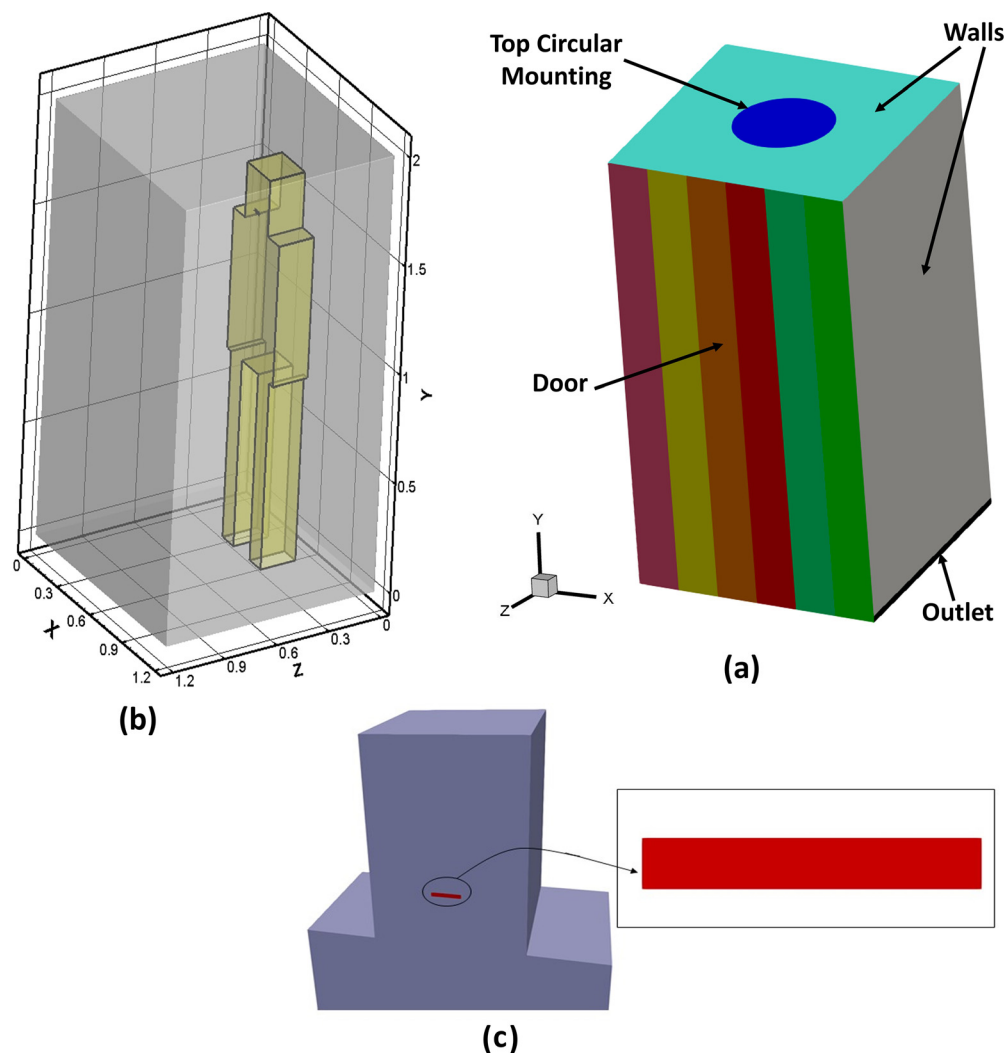


FIG. 1. (a) The whole computational domain. (b) Isometric view of the passenger in the domain. (c) Mouth of the passenger modeled as a rectangular aperture.

TABLE I. Table of scenarios, \hat{j} indicates the positive y direction.

Ambiences	Scenario	Objective	Axial velocity of top circular mounting (m/s)	Angular velocity of top circular mounting (rpm)
Hot dry (30 °C, 50% RH)	1	Effect of quiescent environment	0	0
	2	Effect of axial exhaust	$0.56 \hat{j}$	0
	3	Effect of exhaust fan	$0.56 \hat{j}$	$2000 \hat{j}$
Cold humid (10 °C, 90% RH)	1	Effect of quiescent environment	0	0
	2	Effect of axial exhaust	$0.56 \hat{j}$	0
	3	Effect of exhaust fan	$0.56 \hat{j}$	$2000 \hat{j}$

our desired zone of interest. The passenger height is taken as 1.75 m (the mouth height being 1.56 m).³⁹ Figure 1(b) shows an isometric view of the passenger in the domain, which also shows the position of the passenger relative to the elevator walls. The mouth of the passenger, from which the cough droplets are injected, has been modeled as a rectangularly shaped aperture having a width of 40 mm and an aspect ratio of 8,³⁹ as shown in Fig. 1(c). Three different scenarios have been studied to comprehend the effect of air flow in the surrounding environment on the transmission and evaporation of droplets, injected into the domain by coughing of the passenger. Droplets ejected in the domain due to the coughing of the passenger would traverse the domain, their trajectory being contingent upon the preponderant velocity field. Certain number of droplets could turn into aerosols based on the prevalent temperature and humidity. A number of droplets might escape, a few of them may stick on the various surfaces within the elevator, while the remaining ones will remain suspended in the domain for extended periods—the last ones being of major concern to us.

B. Mathematical model

An Eulerian–Lagrangian model has been implemented for this numerical study. Air, the carrier fluid, is modeled in the Eulerian frame. For the carrier bulk multiphase fluid mixture, the continuity [Eq. (1)]^{29,40} and the compressible multiphase mixture Reynolds-averaged Navier–Stokes equations [Eq. (2)]^{29,40} in conjunction with the k – ω turbulence model in the shear stress transport formulation (SST) [Eqs. (3)–(14)]⁴¹ have been employed. Droplets that are injected into the domain due to coughing are treated as discrete particles and are solved in the Lagrangian frame of reference. The droplets roam around depending on the prevailing air velocity field and undergo evaporation as they traverse the domain. The droplets and moist air at the time of ejection from the mouth can be considered to be at the same temperature as that of the body temperature. Eventually, however, the cloud of droplets intermingles with the surrounding air and it draws in a substantial amount of the surrounding ambient air, following which the temperature of the cloud would effectually be identical to the surrounding ambient temperature.³¹ However, the evaporation process still continues (until the droplet becomes devoid of the volatile component), and the energy required for the phase change to happen is attained from the droplet and the surroundings [Eq. (22)].²⁹ The driving potential for the occurrence of evaporation of water is the difference of partial pressure of the water vapor at the droplet surface and in the air encompassing the droplets [Eq. (27)].²⁹ The rate of

evaporation depends upon the mass transfer coefficient determined from the Sherwood number [Eq. (28)]. The Sherwood number, again, is dependent upon the droplet Reynolds number [Eq. (29)]⁴⁰ based on the Ranz–Marshall correlation [Eq. (28)].^{33,34} The droplet is considered to be a mixture of salt and liquid water (99% water and 1% NaCl wt. %). As the droplets evaporate to lose the volatile liquid mass into the ambient air [Eq. (18)]²⁹ and their diameter decreases, the mass fraction of their components changes [Eqs. (32) and (33)] and finally the droplets fully evaporate, i.e., become fully devoid of the volatile liquid water component, forming droplet nuclei. The droplet properties used in the governing equations are a function of the properties of liquid water and salt as well as their respective mass fractions [Eqs. (34) and (35)]. The continuous change in the mass fractions of these components owing to the evaporation of droplets has been taken into account [Eqs. (31)–(33)]. Hence, to incorporate this salt model of droplets [Eqs. (31)–(36)], modifications have been made in the source code of the reactingParcelFoam solver of OpenFOAM. The Ranz–Marshall model has been implemented to calculate the Nusselt number [Eq. (24)]^{42,43} and Sherwood number [Eq. (28)],^{42,43} to solve the droplet heat transfer [Eq. (22)]²⁹ and mass transfer equations [Eq. (27)].²⁹ The droplet temperature is obtained by solving the energy conservation equation, as discussed below [Eq. (22)].²⁹ The process of evaporative cooling is modeled by taking into account the energy transfer from the bulk phase into the Lagrangian phase [Eqs. (15)–(17) and (23)–(24)].²⁹ The position and the velocity of the droplets are obtained by applying Newton's second law of motion on the droplets, and the forces considered here are gravity, buoyancy, lift, and drag [Eqs. (21), (25), and (26)].^{29,40} The relevant gas phase and particle phase transport equations with appropriate closure relations are as follows:

Governing equations for the Eulerian (gas) phase

Continuity equation,

$$\frac{\partial \rho}{\partial t} + \frac{\partial}{\partial x_j} (\rho u_j) = m_v'''. \quad (1)$$

Momentum equation,

$$\rho \frac{\partial u_i}{\partial t} + \frac{\partial}{\partial x_j} (\rho u_i u_j) = -\frac{\partial p}{\partial x_j} + \frac{\partial \tau_{ij}}{\partial x_i} + \rho g_i. \quad (2)$$

Closure equation for the momentum equation,

$$\tau_{ij} = \mu_t \left(2S_{ij} - \frac{2}{3} \frac{\partial u_k}{\partial x_k} \delta_{ij} \right) - \frac{2}{3} \rho k \delta_{ij}. \quad (3)$$

Strain rate,

$$S_{ij} = \frac{1}{2} \left(\frac{\partial u_i}{\partial x_j} + \frac{\partial u_j}{\partial x_i} \right). \quad (4)$$

Transport equation for turbulent kinetic energy,

$$\frac{\partial(\rho k)}{\partial t} + \frac{\partial(\rho u_j k)}{\partial x_j} = P - \beta^* \rho \omega k + \frac{\partial}{\partial x_j} \left[(\mu + \sigma_k \mu_t) \frac{\partial k}{\partial x_j} \right]. \quad (5)$$

Transport equation for turbulent energy dissipation,

$$\frac{\partial(\rho k)}{\partial t} + \frac{\partial(\rho u_j k)}{\partial x_j} = P - \beta^* \rho \omega k + \frac{\partial}{\partial x_j} \left[(\mu + \sigma_k \mu_t) \frac{\partial k}{\partial x_j} \right]. \quad (6)$$

Turbulent kinetic energy production,

$$P = \tau_{ij} \frac{\partial u_i}{\partial x_j}. \quad (7)$$

Eddy viscosity limiter,

$$\mu_t = \frac{\rho a_1 k}{\max(a_1 \omega, \Omega F_2)}. \quad (8)$$

Weighted model constants,

$$\phi = F_1 \phi_1 + (1 - F_1) \phi_2. \quad (9)$$

Blending function 1,

$$F_1 = \tanh(\arg_1^4). \quad (10)$$

Argument for blending function 1,

$$\arg_1 = \min \left[\max \left(\frac{\sqrt{k}}{\beta^* \omega d}, \frac{500\nu}{d^2 \omega} \right), \frac{4\rho \sigma_{\omega 2} \kappa}{CD_{k\omega} d^2} \right]. \quad (11)$$

Blending function 2,

$$F_2 = \tanh(\arg_2^2). \quad (12)$$

Argument for blending function 2,

$$\arg_2 = \max \left(2 \frac{\sqrt{k}}{\beta^* \omega d}, \frac{500\nu}{d^2 \omega} \right). \quad (13)$$

Constants,

$$\begin{aligned} \sigma_{\kappa 1} &= 0.85, & \sigma_{w1} &= 0.65, & \beta_1 &= 0.075, \\ \sigma_{\kappa 2} &= 1.00, & \sigma_{w2} &= 0.856, & \beta_2 &= 0.0828, \\ \beta^* &= 0.09, & a_1 &= 0.31. \end{aligned} \quad (14)$$

Energy transport from the Lagrangian to Eulerian phase,

$$\rho \frac{\partial H}{\partial t} + \frac{\partial}{\partial x_i} \left[\rho u_i H - \frac{\partial}{\partial x_i} (k_{eff} T) \right] = Q_d. \quad (15)$$

Closure term for the energy equation,

$$H = \sum x_i C_{pi} T_i, \quad (16)$$

$$K_{eff} = k_{mol} + k_t. \quad (17)$$

Species transport equation for water vapor,

$$\frac{\partial(\rho f_v)}{\partial t} + \frac{\partial}{\partial x_i} \left[\rho u_i f_v - \rho D_{eff} \frac{\partial f_v}{\partial x_i} \right] = m_v'''. \quad (18)$$

Closure term for the species transport equation,

$$D_{eff} = D_{mol} + \frac{\nu_t}{Sc_t}, \quad (19)$$

$$Sc_t = 0.7. \quad (20)$$

Governing equations for the Lagrangian phase (droplet properties and parameters subscripted by d)

Equation of motion of droplets,

$$m_d \frac{d\vec{u}_d}{dt} = \frac{\pi d_d^3}{6} (\rho_d - \rho) \vec{g} + \frac{C_d \rho \pi d_d^2}{8} |\vec{u}_d - \vec{u}| (\vec{u}_d - \vec{u}) + \vec{F}_{lift}. \quad (21)$$

Energy conservation equation for the droplet phase,

$$m_d C_{p,d} \frac{dT_d}{dt} = h \pi d_d^2 (T - T_d) + \frac{dm_d}{dt} h_{fg}. \quad (22)$$

Energy transport from the Lagrangian to Eulerian phase,

$$Q_d = \frac{\sum_{i=1}^{i=N} \left(\pi d_{d,i}^2 h (T - T_{d,i}) \right)}{V_{cell}}. \quad (23)$$

Ranz–Marshall correlation for the Nusselt number,

$$Nu = \frac{h d_d}{k_t} = 2.0 + 0.6 Re_d^{0.5} Pr^{0.33}, \quad Pr = \frac{\mu}{\rho \alpha}. \quad (24)$$

Drag coefficient,

$$C_d = \max \left\{ \frac{24}{Re_d} (1 + 0.15 Re_d^{0.687}); 0.44 \right\}. \quad (25)$$

Lift force,

$$F_{lift} = \frac{2K\nu^{0.5} \rho d_{ij}}{\rho_d d_d (d_{ik} d_{kl})^{0.25}} (\vec{u} - \vec{u}_d). \quad (26)$$

Droplet evaporation term,

$$\frac{dm_d}{dt} = \pi d_d^2 m_{wl} k_{mt} \left(\frac{p_{sat}}{RT_d} - X \frac{p}{RT} \right). \quad (27)$$

Ranz–Marshall correlation for the Sherwood number,

$$Sh = \frac{k_{mt} d_d}{D} = 2.0 + 0.6 Re_d^{0.5} Sc^{0.33}. \quad (28)$$

Droplet Reynolds number,

$$Re_d = \frac{d_d \rho |\vec{u}_d - \vec{u}|}{\mu}. \quad (29)$$

Schmidt number,

$$Sc = \frac{\mu}{\rho D}. \quad (30)$$

Mass of nonvolatile components,

$$m_d^s = Y_0^s m_d^0. \quad (31)$$

Mass fraction of nonvolatile components

$$Y_d^s = \frac{m_d^s}{m_d}. \quad (32)$$

Mass fraction of volatile components,

$$Y_d^l = 1 - Y_d^s. \quad (33)$$

Droplet density,

$$\rho_d = \frac{1}{\left(\frac{Y_d^s}{\rho^s}\right) + \left(\frac{Y_d^l}{\rho^l}\right)}. \quad (34)$$

Droplet heat capacity,

$$c_{p,d} = Y_d^s c_{p,s} + Y_d^l c_{p,l}. \quad (35)$$

Droplet diameter,

$$d_d = \left(\frac{6m_d}{\pi\rho_d}\right)^{1/3}. \quad (36)$$

C. Initial and boundary conditions

The top circular mounting is assigned different conditions corresponding to three different scenarios: quiescent, axial exhaust, and exhaust fan. Table I provided below elucidates this further. The two outlets provided at the lower portion of the side walls are defined as pressure outlets with atmospheric pressure. All the walls and the boundary of the passenger are treated as walls with no-slip velocity boundary condition. The door remains closed in all the scenarios; hence, in all these scenarios, the door is modeled as a wall. By conducting numerical simulations, it has been inferred that the initiation time of the cough and air flow development in the domain has significant impact on the droplet kinematics. To eliminate this above-stated bias and to make the situation more representative and generic, the cough is ejected in stages. The complete coughing phenomenon occurs in four stages. As depicted in Fig. 2, the coughing phenomenon commences at 1 s and terminates at 4.12 s. Each single cough occurs for 0.12 s, injecting 1008 droplets of mass 7.7 mg with a velocity of 8.5 m/s normal to the mouth surface.²⁹ In each stream, the initial size distribution of the cough droplets follows the well-known Rosin–Rammler distribution or the Weibull distribution with a scale factor of 80 μm and shape factor of 8.²⁹ The passenger, assumed to be a symptomatic COVID-infected patient, has a comparatively higher body temperature of 38.4 °C. The continuous periodic inhalation and exhalation of the passenger has also been taken into account. The ambient pressure inside the elevator is one atmospheric pressure, 101 325 Pa. The elevator is subjected to two different ambiances: 30 °C, 50% R.H. (hot dry) and 10 °C, 90% R.H. (cold humid). The temperature of the air ejected out of the mouth during exhalation is assumed to be at the body temperature and its relative humidity is assumed to be 100%.²⁹ The injected cough droplets are also at the body temperature. The cough droplets are considered as a mixture of NaCl (salt) and water with initial mass fractions of 0.01 NaCl (solid) and 0.99 water (liquid).⁴⁴

D. Numerical method

The OpenFOAM solver “reactingParcelFoam,” with necessary modifications to successfully implement the salt model as discussed earlier was employed to solve all the required partial differential

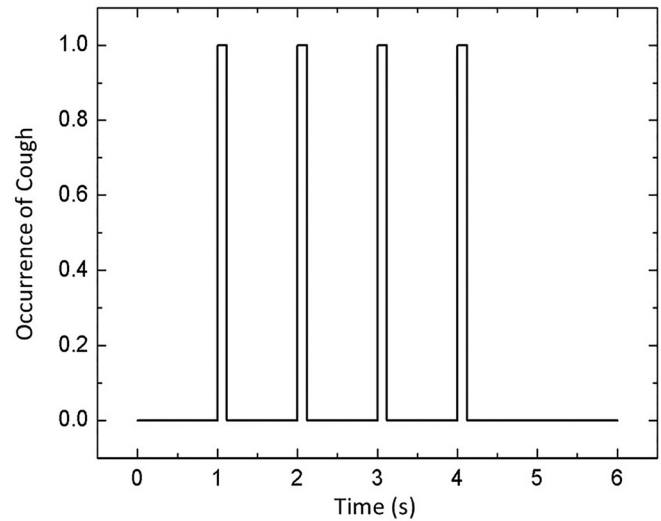


FIG. 2. The entire coughing phenomenon.

equations. It is very important to state that all the thermophysical properties of the Eulerian and Lagrangian phases are functions of temperature. The Eulerian phase has been modeled as an ideal gas for its equation of state, and its transport is modeled using Sutherland’s law⁴⁵ for its viscosity based on the kinetic theory of gases, which is suitable for non-reacting gases. Finite volume methods have been employed to discretize the Eulerian phase. Second-order schemes have been employed for both space and time operators. Semi-implicit numerical schemes of second order have been employed for Lagrangian phase discretization. The grid independence study has been performed, which—to improve the readability of the paper—has been provided in the Appendix.

III. VALIDATION

A. Validation of droplet evaporation model

Although many studies have been conducted, the authors did not take into consideration the effect of soluble components present in the cough droplets. In reality, cough droplets are not pure water and contain dissolved salts (like NaCl) in certain proportions. This presence of salts in cough droplets affects the droplet characteristics in several interconnected ways, as discussed in the Introduction. In our study, an attempt is made to make the simulations more realistic by considering the effect of salt solution in cough droplets, i.e., by including the salt model of droplets. Our model is tested against the reported experimental result of change of diameter of an acoustically levitated 1 wt. % salt (NaCl)-laden droplet with time of Basu *et al.*⁴⁴ For this validation study, only 1 droplet (NaCl 1% wt. %, H₂O 99% wt. %) is injected with initial size of 600 μm at the center of a domain. The quiescent condition is modeled appropriately by taking the domain size to be much larger than the droplet diameter and by assigning the internal field as well as the boundary fields of the entire computational domain a zero velocity. A temperature of 30 °C or 303 K and a relative humidity of 50% is used as reported by Basu *et al.*⁴⁴ In order to model the levitating droplet, the droplet is injected with zero initial velocity and

no force (gravitational, buoyancy or sphere drag) is applied on the droplet, thus keeping it suspended in the domain indefinitely. The droplet diameter reduces continuously owing to its evaporation, and the change in diameter (D) with time is noted. Figure 3(a) compares experimental data (Basu *et al.*⁴⁴) of the temporal history of the instantaneous normalized droplet diameter (D/D_0 , D_0 initial diameter) with our numerically predicted results. The numerically predicted results are in reasonably good agreement with the experimental observations of Basu *et al.*,⁴⁴ as can be seen from the two graphs in Fig. 3(a). Hence, our newly developed droplet salt model is validated.

B. CFD model validation

Before proceeding with the numerical model for our actual study, a quantitative validation of the droplet size distribution is done against the DNS data of size distribution reported by Ng *et al.*¹³ The validation data used are for a temperature of 30 °C and RH of 90%, from Ng *et al.*¹³ For this validation study, the geometry and all the initial and boundary conditions are obtained from Ng *et al.*¹³ The droplet size distribution as predicted by our numerical (CFD) model is compared with the size distribution results of Ng *et al.*¹³ Figure 3(b) compares the droplet size distribution at $t = 0.6$ s. The match between the droplet size distributions is reasonably good. Thus, our numerical (CFD) model is validated and, hence, our numerical (CFD) model along with our newly developed salt model can be used subsequently in our actual study.

IV. RESULTS AND DISCUSSIONS

In this study, two different ambient conditions and three different types of ventilation scenarios in each of the ambient conditions (as summarized in Table I) have been studied.

In the first ambient condition, a hot dry ambience having a temperature of 30 °C and relative humidity of 50% has been investigated, which closely matches the climatic condition of places like Mumbai,

Delhi, New York, and Melbourne in summer. In addition to this, in the second ambient condition, a cold humid ambience having a temperature of 10 °C and relative humidity of 90% found sometimes in places like London, Amsterdam, and Berlin has also been investigated to study the effect of change in environment on droplet transmission. In both the ambient conditions, three different scenarios are studied.

In scenario 1, the effect of a quiescent environment (i.e., no air-flow or ventilation condition) is studied. In scenario 2, the effect of an outward (exhaust) axial jet ventilation condition is studied. In scenario 3, the effect of an exhaust fan ventilation condition is studied. These scenarios have been studied and quantified to progressively move toward a ventilation system that minimizes the chances of getting infected for a passenger/passengers if they had been traveling in the elevator (or is waiting outside to enter the elevator) with the above-mentioned infected passenger considered in the study.

In scenario 1, the effect of a quiescent environment on droplet dynamics and heat transfer characteristics have been studied, whereas scenarios 2 and 3 investigate the effect of forced circulation on the same.

The scenarios 1–3 have been investigated for 10 s, the average time taken by an elevator to traverse 10 floors, considering the average height of a floor as 3 m (complying with National Building Code of India, 2005)^{46,47} and mean elevator speed as 3 m/s.

A. Transport and evaporation of droplets

1. Scenario I

In this scenario, the top mounting is treated as a wall, with no air-flow interaction with the domain, thus making a quiescent environment prevail inside the elevator. For the hot dry case, the droplets do not reach the floor within the stipulated elevator travel time of 10 s, as established by Fig. 4(a) (Multimedia view). It is important to note that droplets do not directly head toward the floor, rather they get

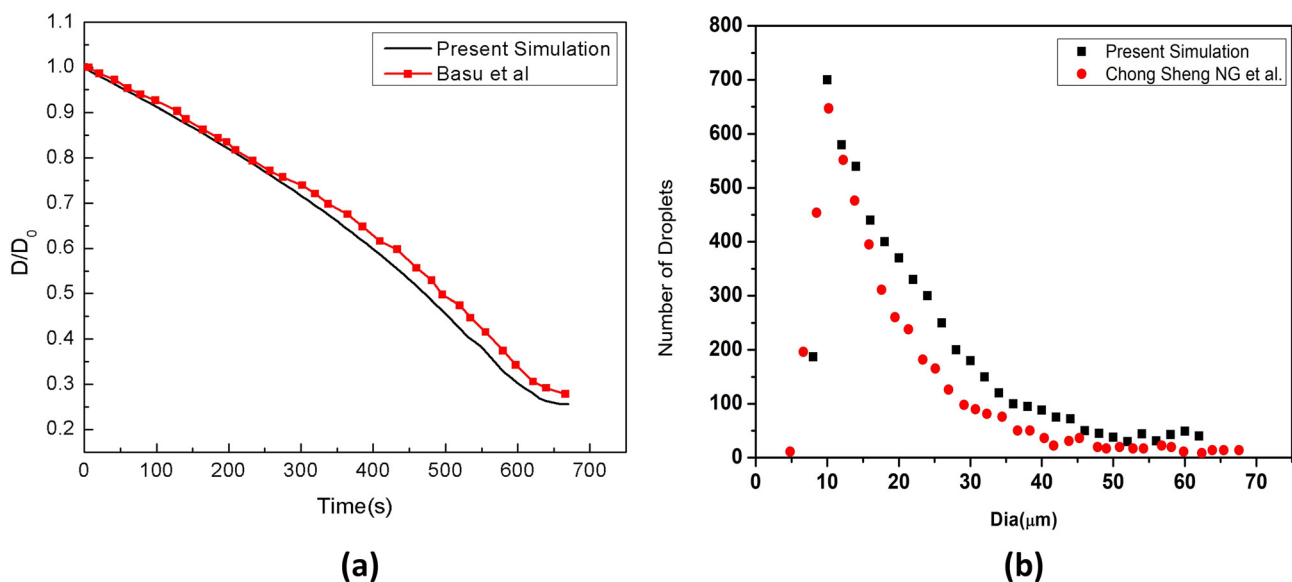


FIG. 3. (a) Validation of droplet evaporation model including crystallization with literature data and (b) validation of droplet size distribution with literature data at $t = 0.6$ s.

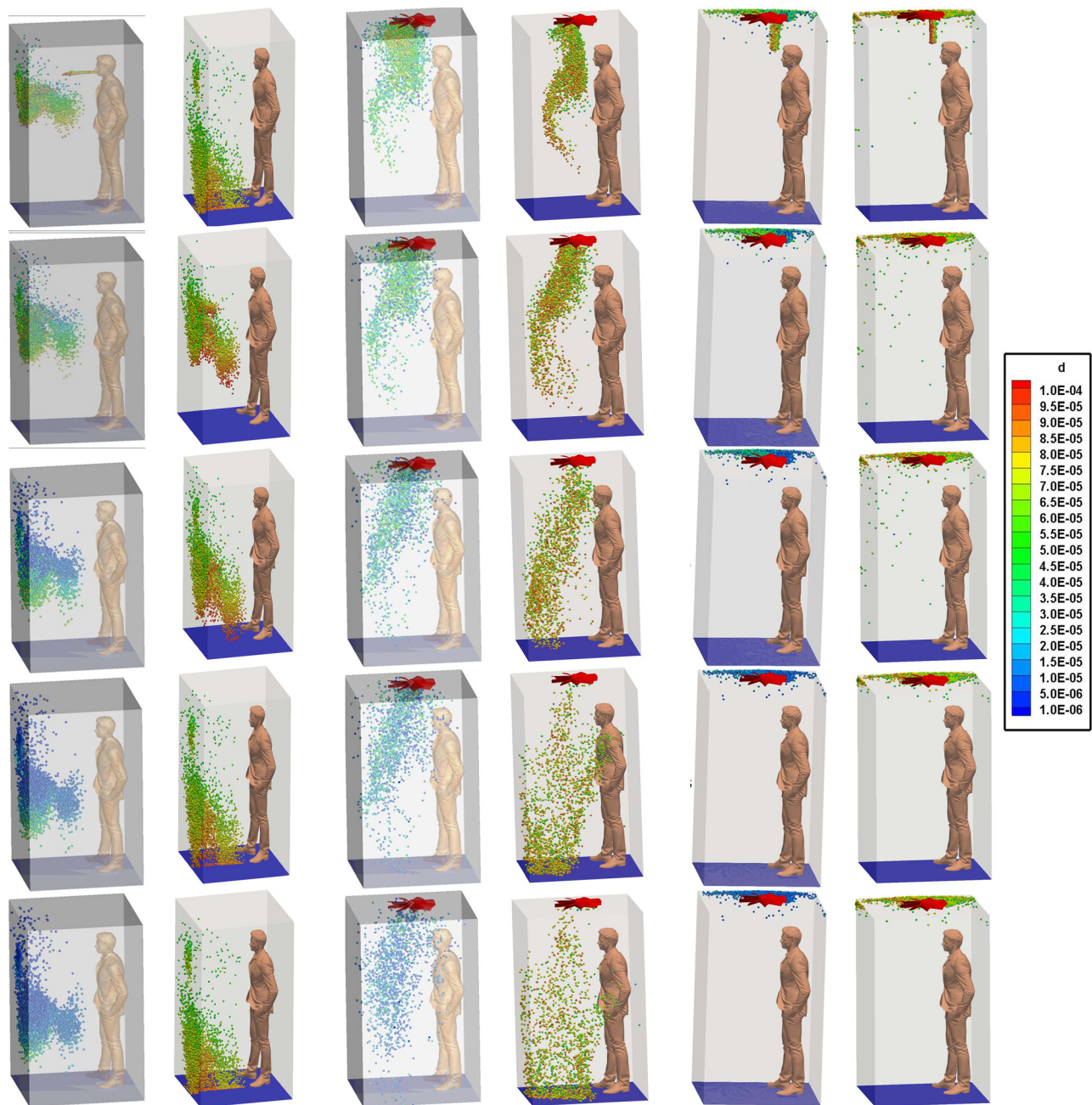


FIG. 4. (a)–(f) Droplet dispersion in the domain at various time instants for all the scenarios of both the ambiances. Multimedia views: <https://doi.org/10.1063/5.0073694.1>; <https://doi.org/10.1063/5.0073694.2>; <https://doi.org/10.1063/5.0073694.3>

entrapped in the turbulence induced both by the cough and the continuous inhalation and exhalation of the passenger, and they get spread across the elevator. The absence of any continuous draft of air in the domain slows down the process of sticking or escaping of the droplets; hence, majority of them remain suspended in the air. The suspended droplets evaporate continuously to decrease in size, as visible from the continuous shrinking size range, depicted by the diameter

distribution of the suspended droplets at various time instances in Figs. 5(a) and 5(b). A probability distribution plot based on the initially injected droplet count has been used to represent the size distribution in Fig. 5. Figure 5 also depicts the probability of droplet nuclei being formed. Droplet nuclei are the droplets from which the volatile liquid component has completely evaporated and is remaining only with the nonvolatile salt component. Due to the initial droplet size

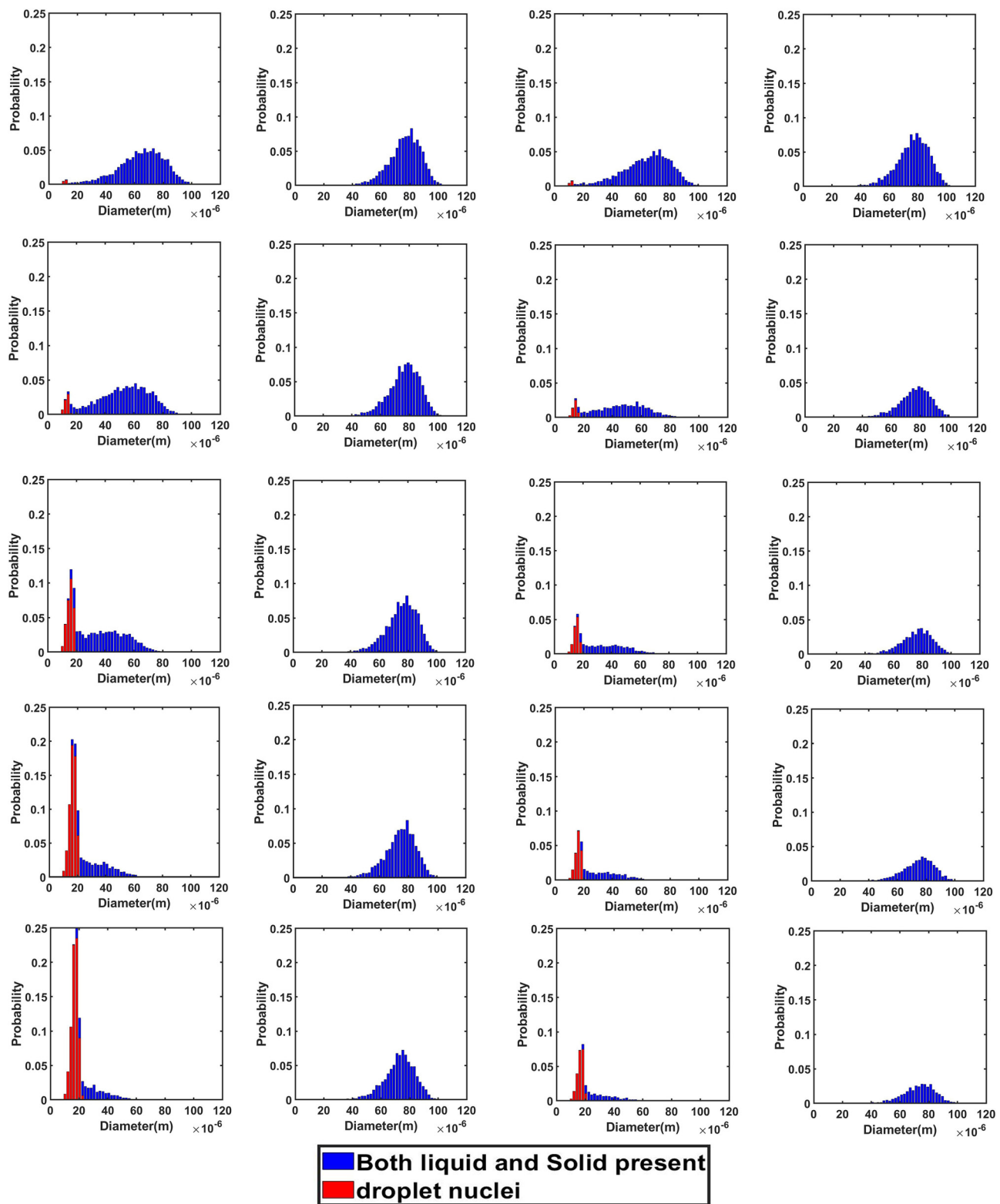


FIG. 5. (a)–(d) Droplet size distribution in the domain at various time instants for all the scenarios of both the ambiances.

distribution following a Rosin–Rammler distribution, we have droplet nuclei of different sizes [Figs. 5(a) and 5(b)] and also it is possible to have a droplet and a droplet nuclei of the same size [Fig. 5(a)]. In this context, it is notable that out of a droplet and a droplet nuclei of the same size, the droplet nuclei is more harmful as it has surely been inherited from an initially larger droplet, thus exhibiting a very high viral load.¹¹ Moreover, the droplet nuclei basically consist of only the nonvolatile component, which in turn contains the pathogen. A significant number of suspended droplets evaporate to form droplet nuclei having sizes mostly in the range of 10–20 μm after 10 s as shown in Fig. 5(a). Droplet nuclei are only found in the hot dry ambience and not in the cold humid ambience, as in the latter there is negligible evaporation, thus preventing the formation of nuclei.

Contrasting results are obtained for the cold humid ambience as shown in Fig. 4(b) as well as from the size distribution at various instants of elevator travel time as can be seen from Fig. 5(b). Due to their relatively large mass as compared to the hot dry condition owing to negligible evaporation, the gravity force dominates over the injected droplets, which ultimately cause the droplets to descend and reach the elevator within the stipulated time of 10 s as can be seen in Fig. 4(b). Moreover, the relatively large diameter due to negligible evaporation, as compared to the hot dry condition, produces a larger drag force on the droplets, which prevents the spread of droplet in the elevator and produces an orderly downward motion. Although a few droplets are initially trapped in the turbulent puff of coughing and spread wayward, owing to the gravity effect and larger drag force, they quickly settle down.

2. Scenario II

In this scenario, the effect of forced circulation in the domain (for both the environmental condition) on droplet dispersion is investigated. Air is drawn out of the domain and the top mounting is modeled as an axial exhaust jet. As can be seen from the droplet distribution [Figs. 4(c) and 4(d) (Multimedia views)], for both the environmental conditions the elevator space (mostly the upper portion) is filled with many suspended particles. This is due to the fact that the first two streams of cough particles move down instead of moving up, while the third and fourth ones move up. This difference occurs because the flow has not developed during the time of injection of the first two streams as depicted by the velocity contours at plane AB (plane AB shown in Fig. 6) of different time instances in Fig. 7, where the development of velocity in the flow field along with the droplets' positions have been depicted for the hot dry ambience. A similar flow pattern is observed for the cold humid ambience. As the flow takes sufficient time to develop as reconfirmed by the temperature contoured velocity vector plots of Fig. 8, for hot dry ambience at plane AB (Fig. 6), the initially injected particles do not receive sufficient drag force to move upward and, hence, descend (due to gravity); but as the flow becomes fully developed, the downward motion of the particles gets arrested and these particles remain suspended in the domain for an extended period of time. As air is drawn out in this scenario, a significant percentage of droplets escapes out of the domain. For the hot dry condition, the suspended droplets evaporate continuously to decrease in size as indicated by the continuously decreasing diameter range of the diameter distributions of the suspended droplets, depicted at various time steps by Fig. 5(c) while majority of the

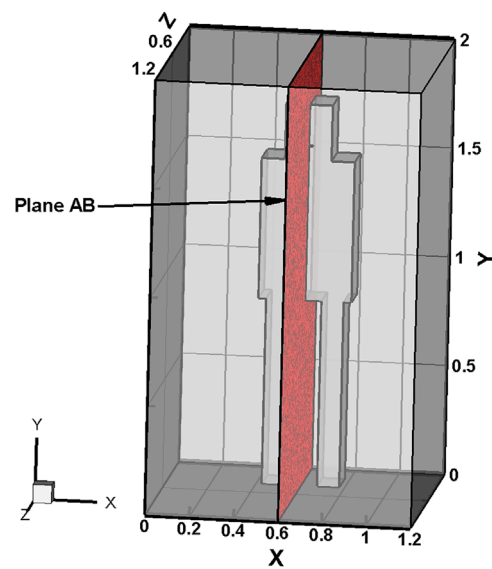


FIG. 6. Cross-sectional plane AB.

suspended droplets turn into droplet nuclei (having size in the range of 10–20 μm) after 10 s. Whereas for the cold humid condition it is found just like the previous scenario, there is negligible evaporation of droplets, preventing the generation of droplet nuclei, Fig. 5(d).

3. Scenario III

In this scenario, the top mounting is modeled as an exhaust fan. Here, the fan rotates with a r.p.m of 2000 to suck air out of the domain. Unlike scenario 2, where the top mounting was modeled as an axial exhaust jet, the rotational effect of fan has also been considered. In contrast with the previous scenario, the flow develops rather quickly in the domain (especially near the man's mouth) to develop a sufficiently strong drag force, for both the ambient conditions as depicted by the temperature contoured velocity vector plots in Fig. 9. This is further elucidated by the velocity contour plots of Fig. 10. Hence, the particles move upward immediately upon injection due to the more enhanced drag force exerted by air on the particles, as can be seen from the droplet dispersion transience depicted in Figs. 4(e) and 4(f) (Multimedia views). The circulation brought about by the rotational effect increases the dispersion in droplet kinematics due to the additional turbulence (created by the rotating component of the fan), due to which the droplets rise up and a significant amount of them gets deposited at the roof (top wall) of the elevator, quite contrary to the previous scenario of axial exhaust jet. As can be understood from the droplet distribution in Figs. 4(e) and 4(f), for the hot dry ambience, after 5.5 s, none of the droplets remain below the height of the passenger, whereas for the cold humid ambience, the elevator becomes safe but it takes 7.48 s. Hence, the domain becomes completely safe from these time instants for both the ambient conditions. Since a negligible percentage of injected droplets remains suspended in the domain at all time instants, the size distribution has not been investigated.

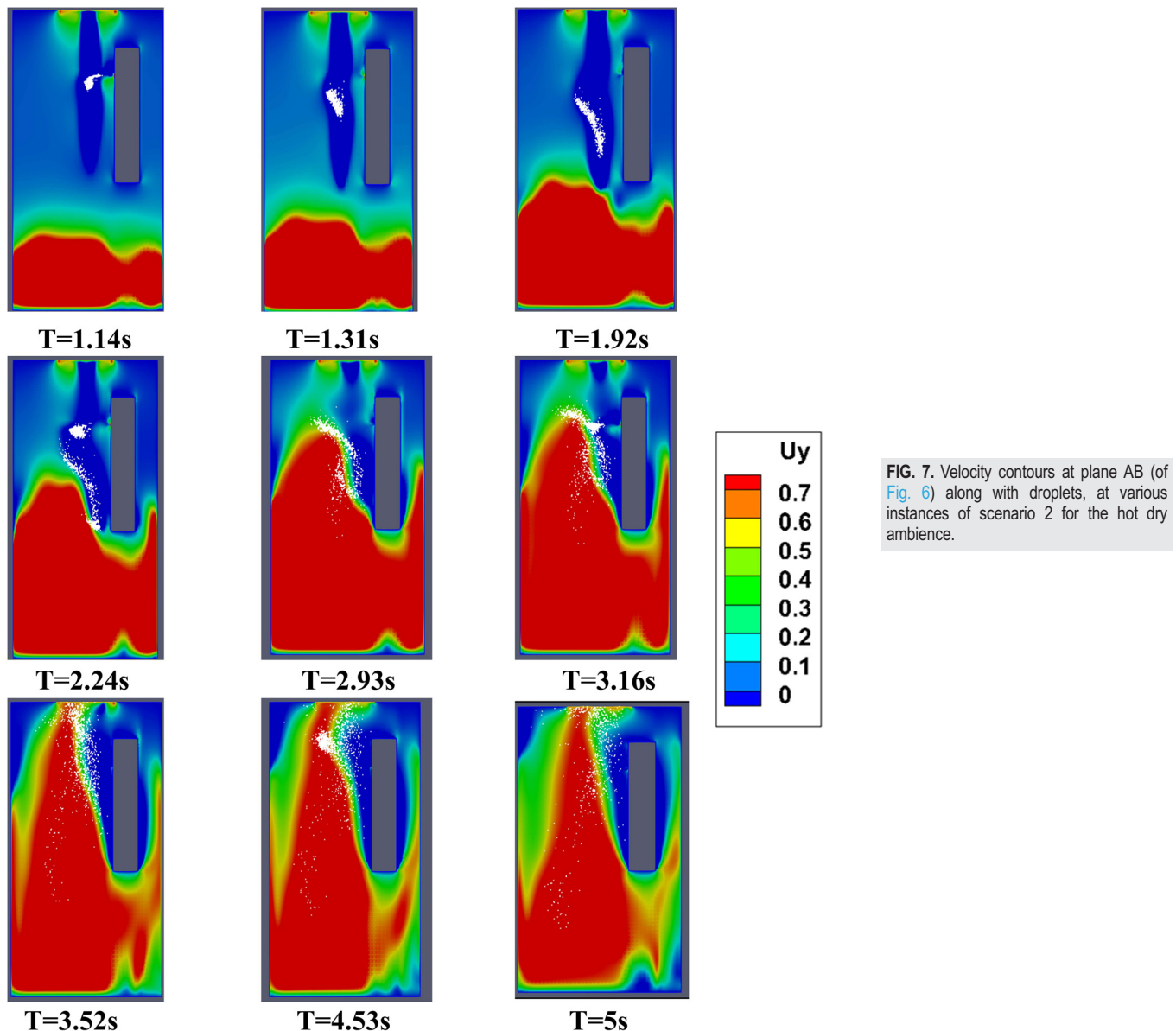


FIG. 7. Velocity contours at plane AB (of Fig. 6) along with droplets, at various instances of scenario 2 for the hot dry ambience.

B. Implications for spread of disease

It is a critically acclaimed fact that the two main modes of spread of coronavirus are by touch and inhalation of particles having significant viral load. So, it is critical that we investigate how the dispersed droplets in the domain might come in contact with a person and obtain a better understanding of this aspect. At first, it is important to quantify how the droplets disperse in the domain by enumerating the percentage of injected droplets that remains suspended in the domain, that escapes from the domain, and that gets deposited on the elevator surfaces. The height range 0.8–1.8 m (average height from a person's waist to head) is identified as the risky height zone, as droplets (either suspended or deposited on surfaces) in this zone will be most perilous

to any other person traveling in the elevator—as these droplets may be directly inhaled by the other passengers. Figure 11 shows the percentage of injected droplets that remains suspended in the domain (within and outside the risky height zone), the percentage that escapes, and the percentage of droplets that gets deposited within and outside the risky height zone on the elevator surfaces, for the various scenarios. A parameter called risk factor is defined as the time-averaged percentage of injected particles that remains suspended in the domain within the risky height zone over an inhalation time period and this parameter is an indicator of the probability of an exposed passenger to get infected. The period of averaging being a typical inhalation cycle of 1 s, within this time span of 1 s, the values of percentage of injected droplets in

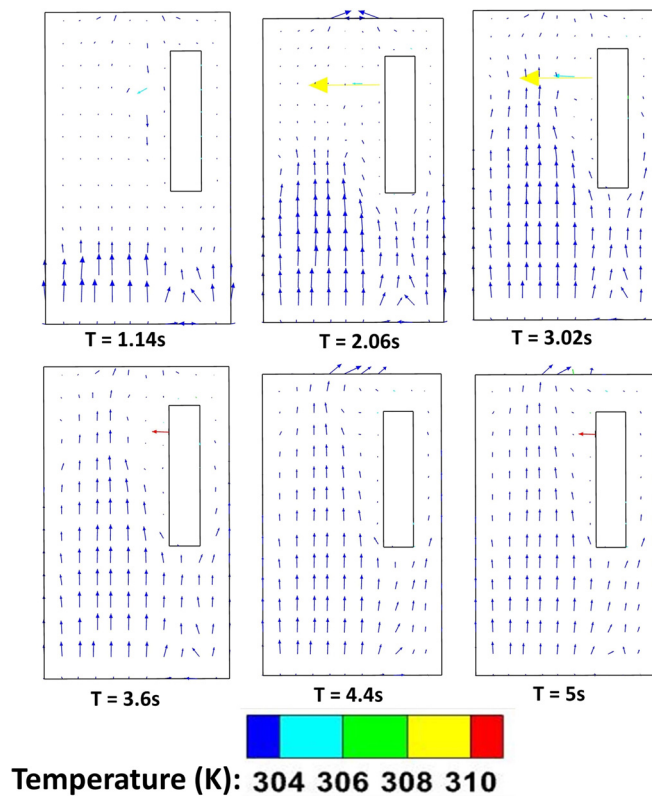


FIG. 8. Temperature contoured velocity vector plots at plane AB (of Fig. 6) at different time instances, of scenario 2 for the hot dry ambience.

the risky height zone at five different instants have been computed. Our defined risk factor is the average of these values. In the bottom right corner of Fig. 12, five instantaneous values of percentage of droplets suspended in the risky height zone (in black) and the average of these instantaneous values representing the defined risk factor for the

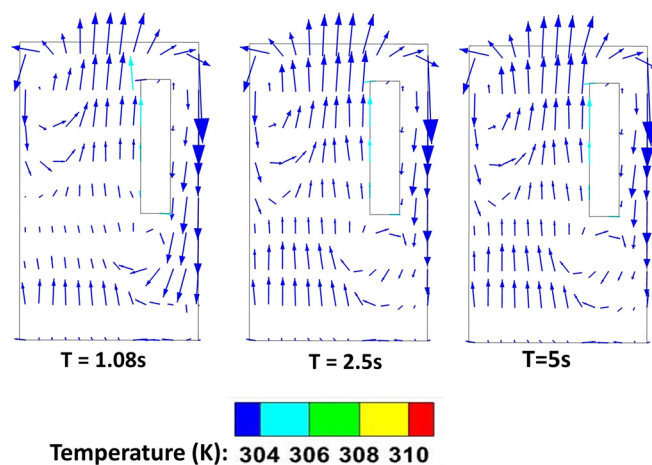


FIG. 9. Temperature contoured velocity vector plots at plane AB (of Fig. 6) at different time instances, of scenario 3 for the hot dry ambience.

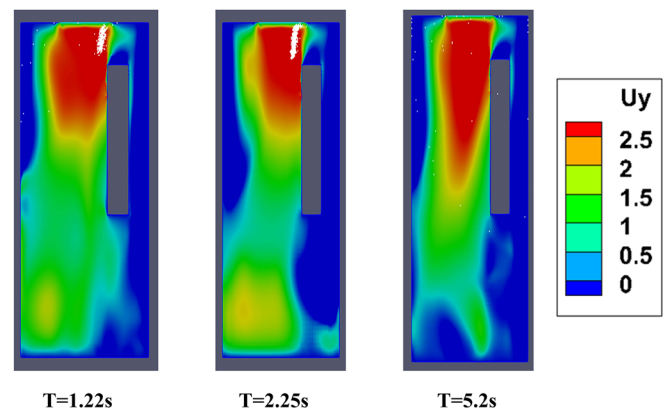


FIG. 10. Velocity contours at plane AB (of Fig. 6) along with droplets, at various instances of scenario 3 for the hot dry ambience.

period of 6–7 s (in red) have been depicted (for one particular representative of cold humid quiescent scenario) in order to elucidate the above-mentioned averaging process. These risk factors have been depicted at different time instants for the different scenarios in Fig. 12. It is understood from Figs. 11 and 12 that in a quiescent domain with hot dry condition, where there is no continuous draft of air, almost all the droplets remain suspended in the domain and only a small percentage gets deposited on the surfaces. Moreover, a fair percentage of suspended droplets remains in the risky height zone at all times (Fig. 12), thus producing the highest risk factor of all the scenarios, rendering a bleak future to the elevator and its other passengers. In contrast, for the cold humid ambience the droplets settle below the risky height zone owing to their larger masses at latter stages of the stipulated time, bringing down the risk factor significantly below that of a hot dry ambience as shown in Fig. 12.

The introduction of a forced circulation of air in the form of axial exhaust jet alleviates the problem for hot dry ambience and produces a significant change in droplet dynamics, as can be seen from Fig. 11, by significantly reducing the percentage of droplets that remains suspended in the domain and increasing the percentage of droplets that escapes out of the domain. The first and second streams of droplets move downward initially due to the force of gravity (which is not balanced by the weak drag force), thus ultimately contributing to producing a high-risk situation. As the flow gets developed in the domain, the third and fourth stream of droplets go up, whereas the droplets from the first two streams remain suspended in the domain due to the stronger drag force now available due to complete the development of the flow.

Although this situation produces a significant amount of risk in the domain, since a significant percentage of the third and fourth stream droplets escapes out of the domain, the situation improves as compared to the quiescent scenario producing a lower risk as compared to the quiescent scenario. On the contrary, for the cold humid ambience, although the axial exhaust scenario initially ameliorates the situation as compared to the quiescent scenario, at later stages the risk associated with the quiescent scenario falls below that of the axial exhaust as depicted in Fig. 12. In this case of axial exhaust jet as discussed, the flow takes some time to develop and the droplets remain suspended in the domain, thus producing a higher risk at later stages

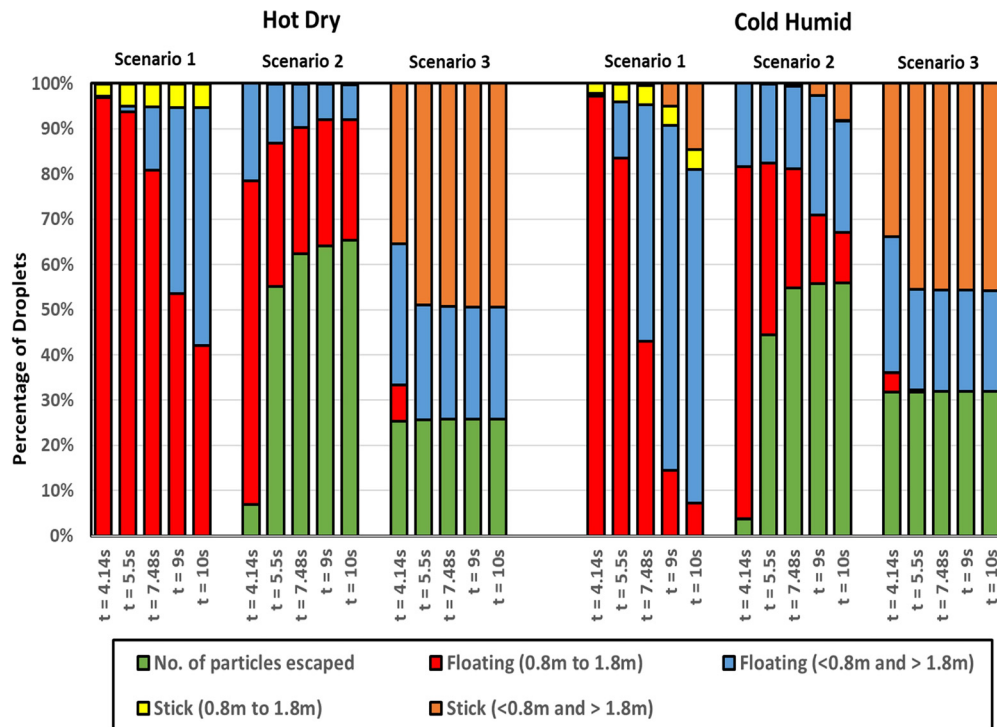


FIG. 11. Droplet fate at various time instants for all the scenarios of both the ambiances.

as compared to the quiescent scenario where the droplets ultimately settle down below the risky height zone owing to their larger diameter due to reasons discussed earlier. Additionally, it is found from Fig. 4(d) that in the cold humid ambience, a significant percentage of the initially injected large droplets quickly falls below the risky height zone owing to larger masses and negligible evaporation. This causes the risk factor for this scenario in cold humid ambience to be below the hot dry ambience, as can be understood from Fig. 12.

In the third scenario, the top mounting has been modeled as the exhaust fan by taking into account its rotation. This ventilation condition is the best solution for ensuring minimum risk as compared to

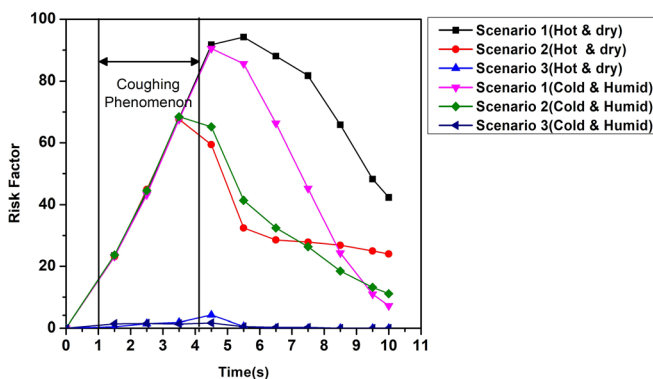


FIG. 12. Risk factor for various scenarios along with the elucidation of the time averaging process for the computation of risk factor in the bottom right corner.

the others. The circulation brought about by the rotational effect increases the dispersion in droplet kinematics due to the additional turbulence (created by the rotating component of the fan) as can be understood from the velocity contour plots of Fig. 10 due to which the droplets rise up and a significant amount of them gets deposited at the roof (top wall) of the elevator, quite contrary to the previous scenario of axial exhaust jet. The risk for this scenario remains approximately equal and significantly low for both the ambiances at all instants. Furthermore, it is found that after 5.5 s for the hot dry scenario and 7.48 s for the cold humid ambience, there are no droplets in the risky zone; hence, there is no risk of being infected. That more time is required for the cold humid ambience is understandable due to larger masses of droplets owing to negligible evaporation. Thus, it can be concluded that the exhaust fan ventilation condition is the best solution for minimizing the risk of infection in elevators. Moreover, it is understood for all other ventilation scenarios that a hot dry ambience poses a higher risk as compared to a cold humid ambience.

So far, we have emphatically established the fact that out of all the ventilation scenarios, scenario 3 is the best-case scenario, as after some time there remains no droplet in the risky height zone, making the domain completely safe, and the risk falls down to zero. However, it is also important to note that if any of the other scenarios are being used as ventilation conditions in an elevator, the safe radial distances to be maintained from the mouth of the infected passenger to ensure maximum safety in the elevator must also be investigated. Hence, first, the height of each suspended droplet in the domain has been tracked at the end of 10 s as shown in Figs. 13(a)–13(f), and, second, among these suspended droplets, the radial distance of those droplets

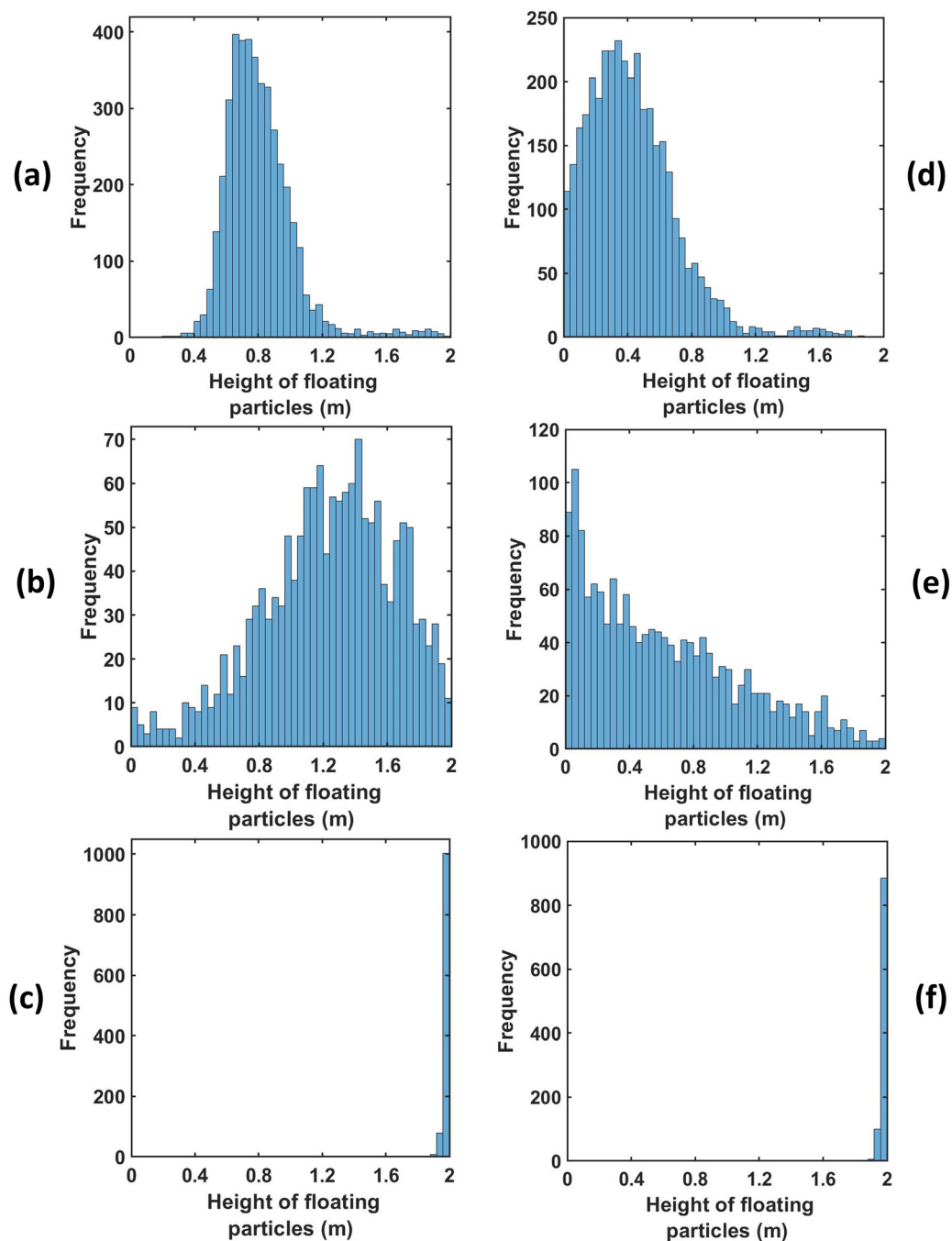


FIG. 13. (a)–(f) Height distribution of suspended particles for various scenarios of both the ambiances at the end of 10 s.

suspended in the risky height zone has been tracked, as depicted in Figs. 14(a)–14(d), to ascertain the minimum radial distance to be maintained in all the cases to avoid coming in contact with any droplet in the risky height zone as much as possible. The safe distances for all scenarios for both ambiances are enumerated in Table II. For both, the

quiescent scenario requires maintaining the maximum radial distance from the passenger's mouth to get rid of the palpable danger pervading the elevator domain. In fact, for the cold humid ambiance, droplets are present at the farthest possible distance from the passenger's mouth. Except scenario 3, where the domain gets completely safe quickly, the

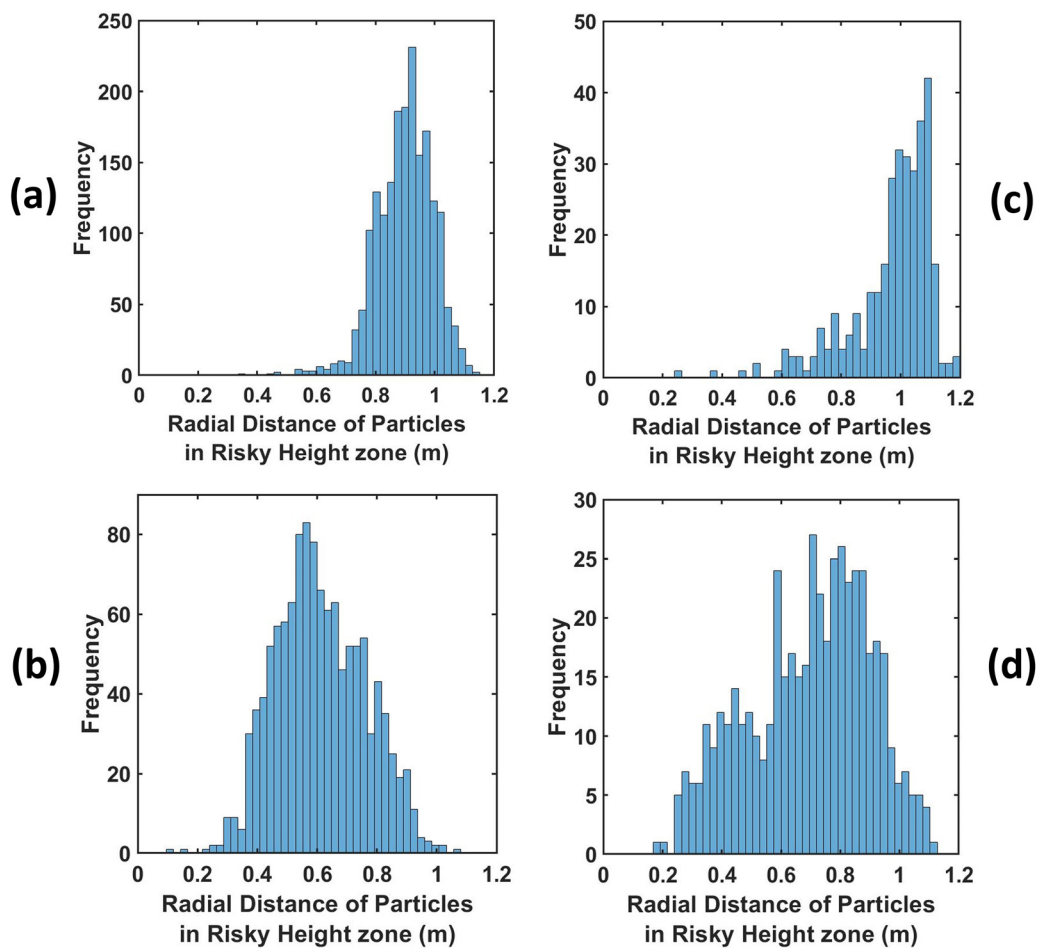


FIG. 14. (a) and (b) Radial distance distribution in the risky height zone for the quiescent and axial exhaust scenarios of the hot dry ambience at the end of 10 s. (c) and (d) Radial distance distribution in the risky height zone for the quiescent and axial exhaust scenarios of the cold humid ambience at the end of 10 s.

cold humid ambience requires one to maintain a greater radial distance for complete safety as compared to a hot dry ambience.

Another important fact that was investigated was the rate of evaporation of the suspended droplets in the domain—indicated by the rate of formation of droplet nuclei from the suspended droplets. This is only applicable for the hot dry ambience, as there is negligible

evaporation in the cold humid scenario. It is important to understand that these droplets will continuously evaporate to form very small-sized particles that will remain suspended in air for a very long duration and will have a high chance of infecting any other person traveling in the elevator. Figure 15 shown below depicts the percentage of suspended droplets that have fully evaporated to form droplet nuclei at different time instances for various scenarios. It can be seen for the forced circulation scenario of exhaust fan that the evaporation rate is higher than that of quiescent scenario (scenario 1). This is because, in the scenario of exhaust fan, the increased velocity of the droplets increases the evaporation rate owing to the increased Sherwood number for the droplets. Moreover, there is an increased dispersion of droplets in the elevator due to the additional turbulence brought about by the rotation of the fan. However, in the case of axial exhaust jet (although it is a forced circulation scenario), the evaporation rate is slower as compared to the other scenarios, because it takes significant amount of time for the flow to develop and droplet cloud from the first two streams travel together in a cluster, remaining condensed (and suspended) rather than spreading across the domain and hence

TABLE II. Safe radial distances for various scenarios.

Ambience	Scenario	Distance (m)
Hot dry	Scenario 1	1.1312
	Scenario 2	1.0682
	Scenario 3	Entire domain is safe
Cold humid	Scenario 1	1.2
	Scenario 2	1.13
	Scenario 3	Entire domain is safe

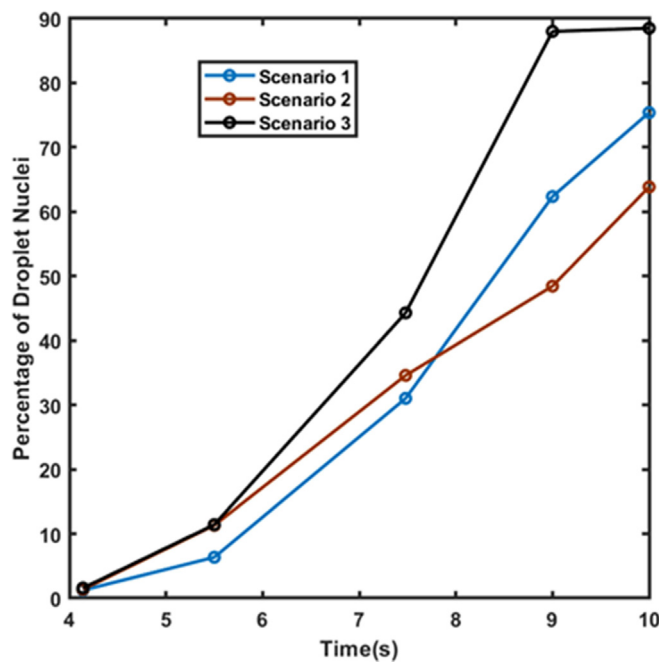


FIG. 15. Percentage of suspended droplets that have fully evaporated to droplet nuclei at different time instances for various scenarios for the hot dry ambience.

residing in areas having a locally higher concentration of water vapor, thereby slowing the evaporation rate. Nevertheless, we can say that a significant fraction of suspended droplets gets fully evaporated to droplet nuclei at a fairly fast rate. This high evaporation rate is a matter of concern, as a significant percentage of injected droplets quickly evaporates to form virusols, i.e., particles having very high viral load and diameter less than $20\text{ }\mu\text{m}$ that remain suspended in the domain for a long period of time.⁴⁸ These virusols are the most dangerous of all the droplets. Due to their size ($\text{dia} < 20\text{ }\mu\text{m}$), they have the highest penetration in human lungs.⁴⁹ A comparison of the percentage of injected droplets that have formed suspended virusols in the risky height zone at different time instants is shown in Fig. 16 below for the hot dry ambience. The virusol count is negligible (close to zero) for cold humid conditions owing to negligible evaporation. Scenario 1 (hot dry ambience) has the highest concentration of virusols suspended in the risky height zone (Fig. 16), thus aggravating the threat of infection inside elevators. Figures 17(a)–17(d) portrays the size range of the droplets suspended in the risky height zone after 10 s, thus giving an idea of the viral load residing in this regime; it also tracks the droplets' radial locations and their concentration in a single plot, for scenarios 1 and 2 (since in scenario 3 no droplets remain after 5.5 or 7.48 s in the domain for both the ambiances). Figures 18(a) and 18(b) extract out the virusols (for cold dry ambience) and show separately the radial concentration of these virusols suspended in the risky height zone, i.e., the number of virusols suspended at different radial locations from the mouth, and thus give an idea of the most critical radial distance, i.e., the radial distance having the highest concentration of malicious virusols. The most critical (or the most dangerous) radial distance for the different scenarios (of hot dry ambience) is enumerated in Table III. This most critical radial distance must always be

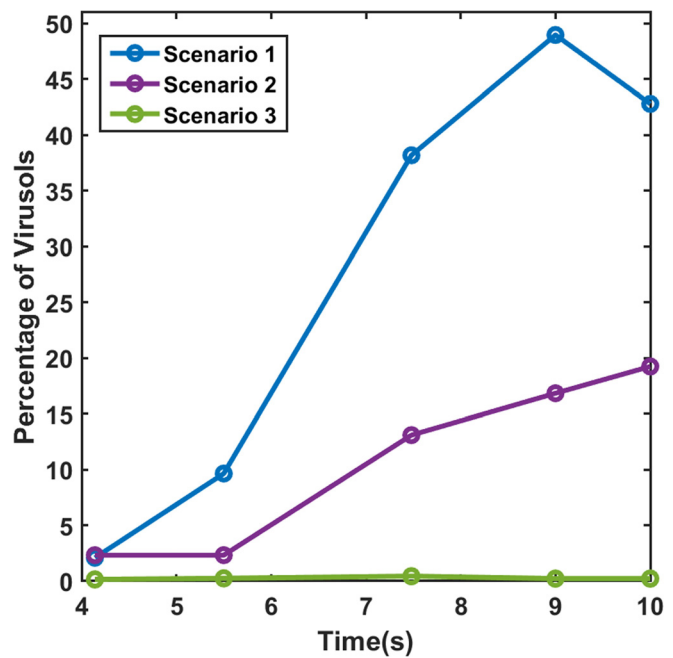


FIG. 16. Percentage of suspended virusols in the risky height zone at different time instances for various scenarios for the hot dry ambience.

avoided by the other passengers to somewhat avert the chances of infection.

V. CONCLUSION

The transmission and evaporation of injected droplets in an elevator typically used in multistoried residential or small enterprise buildings have been modeled. Three ventilation scenarios, viz., quiescent, axial exhaust, and exhaust fan, have been simulated within the elevator. As the droplets move according to the prevailing ventilation patterns, their evaporation is affected by the prevailing air, velocity, temperature, and humidity. In these investigations, various scenarios have been explored to understand the droplet dynamics in the domain.

The simulation results show that a quiescent condition in the elevator has a very high risk associated with it, as a significantly large percentage of droplets remains suspended in the domain in the risky height zone (0.8–1.8 m), especially for the hot dry condition. For the cold humid condition, the droplets settle below the risky height zone at later stages due to their larger masses, owing to negligible evaporation in such an ambience, thus bringing down the risk significantly. Hence, the quiescent scenario turns out to be safer for the cold humid ambience (risk factor 7.22%, at 10 s) as compared to the hot dry ambience (risk factor 40.32% at 10 s). The introduction of forced circulation ventilation in the form of axial exhaust jet or exhaust fan alleviates the situation by bringing down the risk factor as compared to a quiescent scenario. This is attributed to the fact that, with the introduction of forced circulation, the percentage of droplets escaping out of the domain increases significantly. Although the axial exhaust jet fully alleviates the situation for hot dry conditions (risk factor 24% at 10 s) as compared to the quiescent scenario, the cold humid ambience

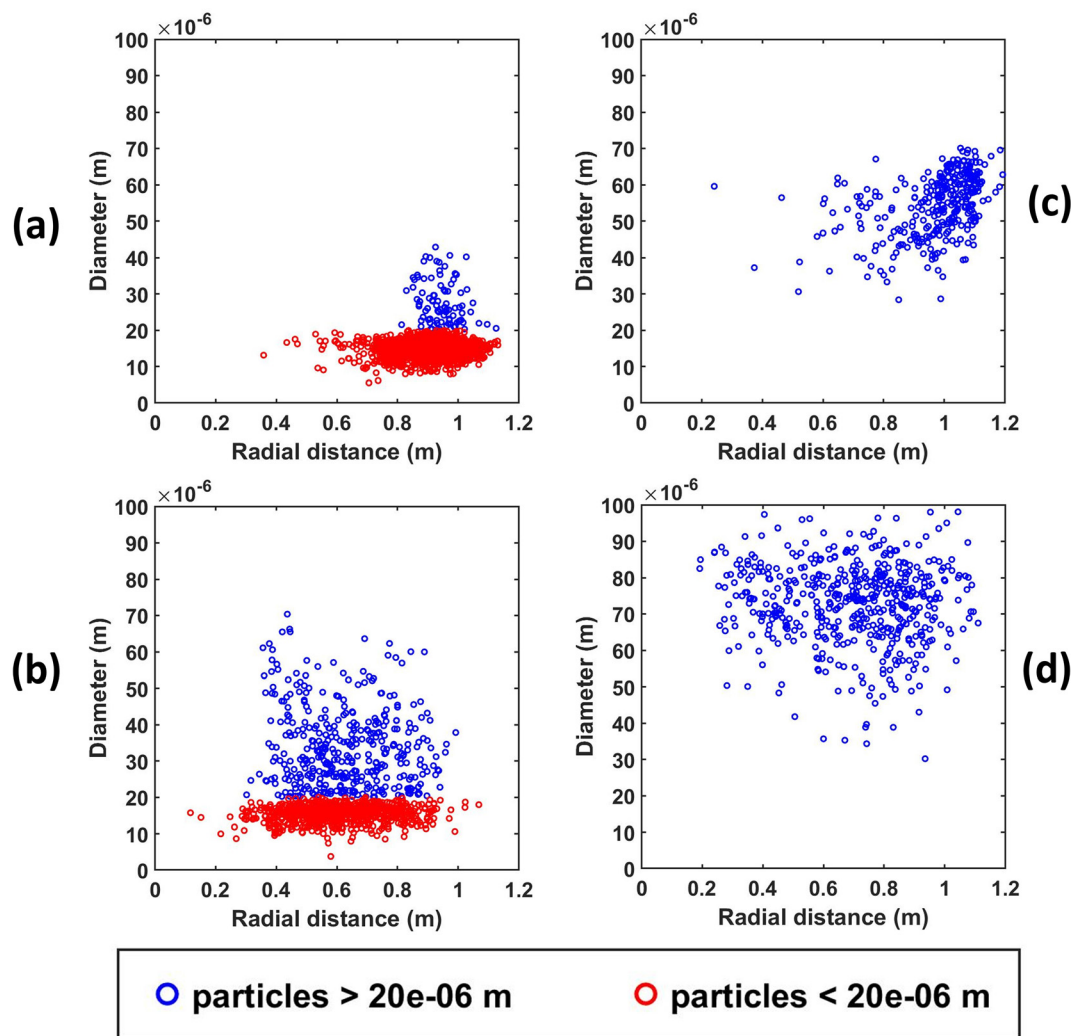


FIG. 17. (a)–(d) Radial location tracking and diameter of the suspended particles in the risky height zone after 10 s, for different scenarios of both the ambiances.

produces different results. As the flow takes some time to develop in these cases for both the ambiances, the initially injected droplet streams go downward due to gravity, which dominates over the upward pulling weak drag force; but, as the flow gets developed the droplets remain suspended in the risky height zone due to the now present stronger drag force, whereas the droplets in the quiescent scenario with cold humid ambience settle down below the risky height zone at latter stages of elevator travel, bringing down the risk (risk factor 7.22%). Furthermore, it has been found that the risk in the exhaust jet scenario is less in the cold humid ambience than the hot dry ambience. The introduction of exhaust fan alleviates the situation for both the ambiances. The risk factor is significantly low for both the ambiances at all time instants, and after 5.5 and 7.48 s no droplets remain in the risky height zone for both the hot and cold ambiances. Hence, it is concluded that the use of exhaust fans is the best solution for

mitigating infection. Moreover, it is found for all the ventilation scenarios that the cold humid ambience is safer as compared to the hot dry ambience.

Although the forced circulation ventilation scenarios mitigate the risk factor more significantly than the quiescent scenario, in general, for forced circulation scenarios, the increased air velocity expedites the evaporation process of the droplets and the increase in turbulence of flow causing dispersion of droplets into areas having lesser mass fraction of water vapor also contributes to the increased evaporation rate especially for the hot dry ambience. The cold humid ambience produces negligible evaporation for all the ventilation scenarios. The increased evaporation rate increases the percentage of virusols among the suspended droplets. These virusols (diameter $< 20\mu\text{m}$), besides having very high viral loading, also have the largest penetration in human trachea. The most critical radial distance (i.e., the radial

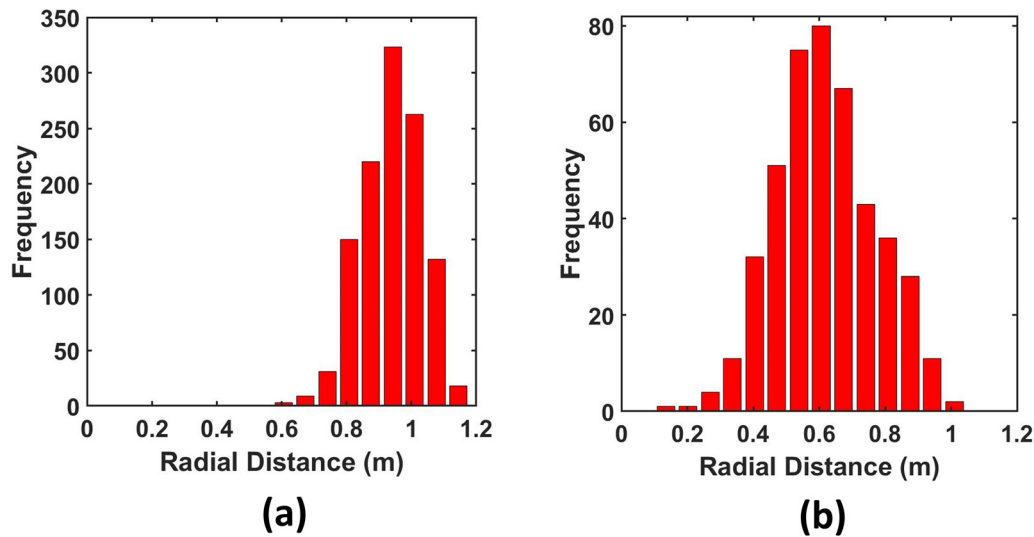


FIG. 18. (a) and (b) Radial distribution of virusols suspended in the risky height zone after 10 s, for different scenarios of the hot dry ambience.

TABLE III. The most critical radial distance for various scenarios, for the hot dry ambience.

Scenario	Distance (m)
Scenario 1	0.95
Scenario 2	0.6
Scenario 3	Entire domain is safe

distance having the highest concentration of virusols) for various scenarios is also obtained from our study. Other fellow passengers inside the elevator must always try to avoid this critical radial distance.

It is important to understand that the scenarios that have been considered in this study are merely a fraction of a plethora of such likely real-life instances where the dimensions of the elevator, air supply and outflow slots, location of a fan or exhaust fan, velocity and speed, and total time of elevator travel may be different from what are considered in this study. The passenger height and his/her positions within the elevator may also differ. The results are expected to be significant for these parametric variations and some of these situations may also present a substantial amount of threat in addition to the ones shown. Therefore, it is exhorted to take utmost precautionary measures while using an elevator.

ACKNOWLEDGMENTS

We would like to thank the high-performance computing cluster in the Technological Bhavan of Jadavpur University for allowing us to execute the simulations within a reasonable time period.

AUTHOR DECLARATIONS

Conflict of Interest

The authors declare that there is no conflict of interest.

DATA AVAILABILITY

The data that support the findings of this study are available from the corresponding author upon reasonable request.

NOMENCLATURE

C_d	Coefficient of drag
C_p	Specific heat capacity of the Eulerian phase (air) ($\text{J kg}^{-1} \text{K}^{-1}$)
$C_{p,d}$	Specific heat capacity of the droplet ($\text{J kg}^{-1} \text{K}^{-1}$)
$C_{p,s}$	Specific heat capacity of the nonvolatile component of droplets ($\text{J kg}^{-1} \text{K}^{-1}$)
$C_{p,l}$	Specific heat capacity of the volatile component of droplets ($\text{J kg}^{-1} \text{K}^{-1}$)
d_d	Diameter of the droplet (m)
D_{eff}	Effective diffusivity ($\text{m}^2 \text{s}^{-1}$)
D_{mol}	Molecular diffusivity in air ($\text{m}^2 \text{s}^{-1}$)
f_v	Mass fraction of water vapor in the Eulerian phase
F_{lift}	Lift force on droplets (N)
h	Convective heat transfer coefficient ($\text{W m}^{-2} \text{K}^{-1}$)
H	Enthalpy (J kg^{-1})
h_{fg}	Latent heat of vaporization of the droplet (J kg^{-1})
k	Turbulent kinetic energy (J kg^{-1})
k_t	Thermal conductivity ($\text{W m}^{-1} \text{K}^{-1}$)
k_{mt}	Mass transfer coefficient for the droplet (m s^{-1})
m_d	Mass of droplet (kg)
m_{wl}	Molecular weight of the volatile component in droplets (kg)
m_d^0	Initial mass of the droplet (kg)
Nu	Nusselt number
p	Static pressure of the Eulerian phase (N m^{-2})
P	Turbulent kinetic energy production ($\text{N m}^{-2} \text{s}^{-1}$)
RH	Relative humidity (percentage)
Sh	Sherwood number

t	Time (s)
T	Temperature (K)
T_d	Temperature of the droplet (K)
\vec{u}	Velocity of the Eulerian phase (ms^{-1})
\vec{u}_d	Velocity of the droplet (ms^{-1})
Y_d^s	Mass fraction of the nonvolatile component of droplets
Y_d^l	Mass fraction of the volatile component of droplets
Y_0^s	Initial mass fraction of the nonvolatile component of droplets
μ	Dynamic viscosity of the Eulerian phase ($\text{kg m}^{-1} \text{s}^{-1}$)
μ_t	Turbulent viscosity of the Eulerian phase ($\text{kg m}^{-1} \text{s}^{-1}$)
ρ	Density of the Eulerian phase (kg m^{-3})
ρ_d	Density of the droplet (kg m^{-3})

APPENDIX: DETAILED GRID INDEPENDENCE STUDY

Grid Independence Study

A 3D structured hexahedral-dominant mesh is used for the discretization of our computational domain. The mesh consists of approximately 5.8×10^5 cells. Mesh refinement is applied near the top mounting, outlets as well as other boundaries, but most importantly, sufficient refinement is applied near the passenger's mouth, from which the cough droplets are injected, to capture the droplet motion accurately. A smooth and gradual transition was also made from the very refined mesh near the mouth to the ambient mesh. A thorough grid independence study was conducted before selecting the above mesh. Three different mesh sizes, viz., coarse (454 327 cells),

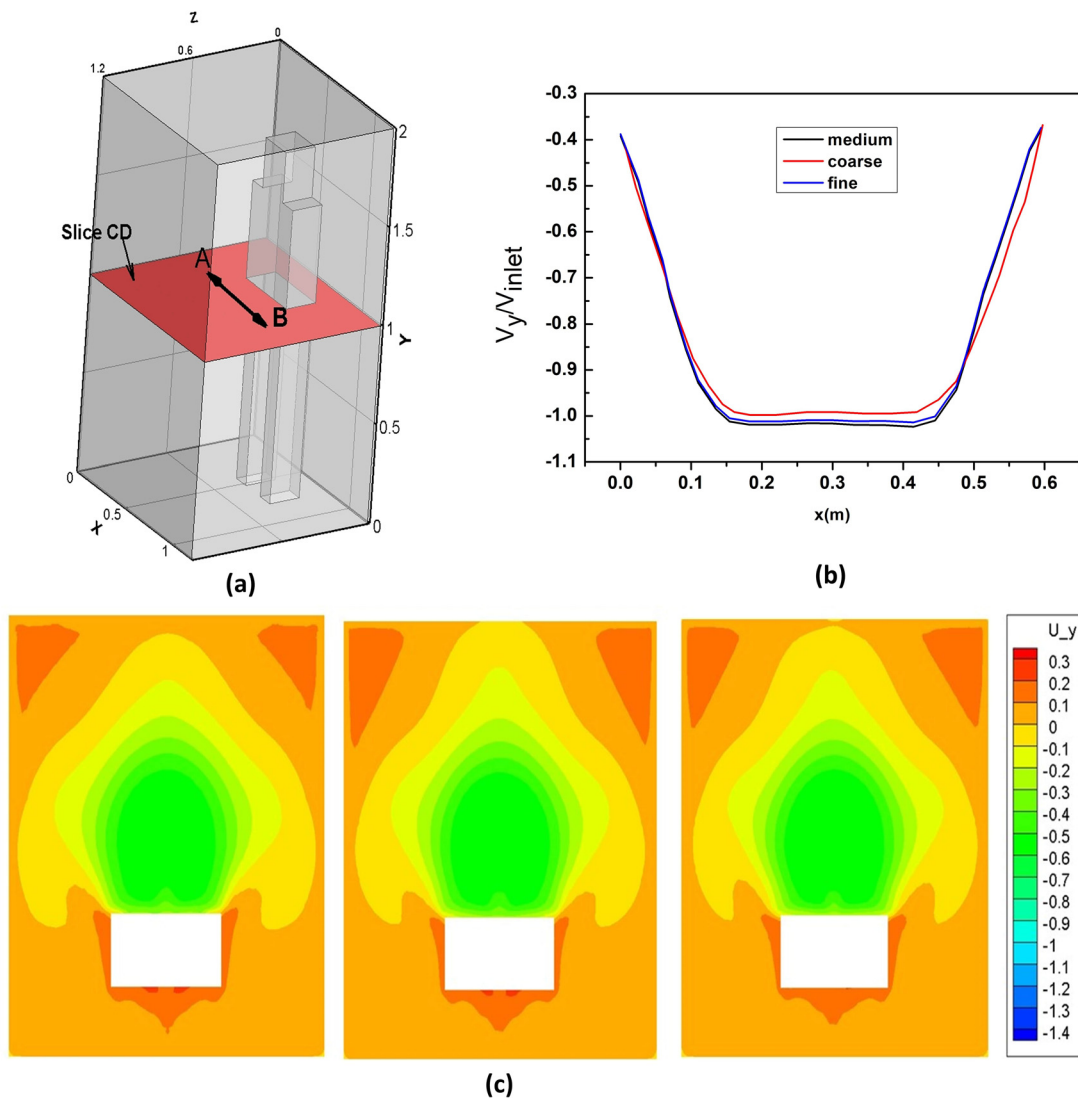


FIG. 19. (a) Location of slice CD and line AB. (b) Comparison of velocity profile (V_y) of different mesh sizes at line AB. (c) Comparison of velocity contours of different mesh sizes at slice CD for coarse, medium, and fine mesh sizes, respectively, from left to right.

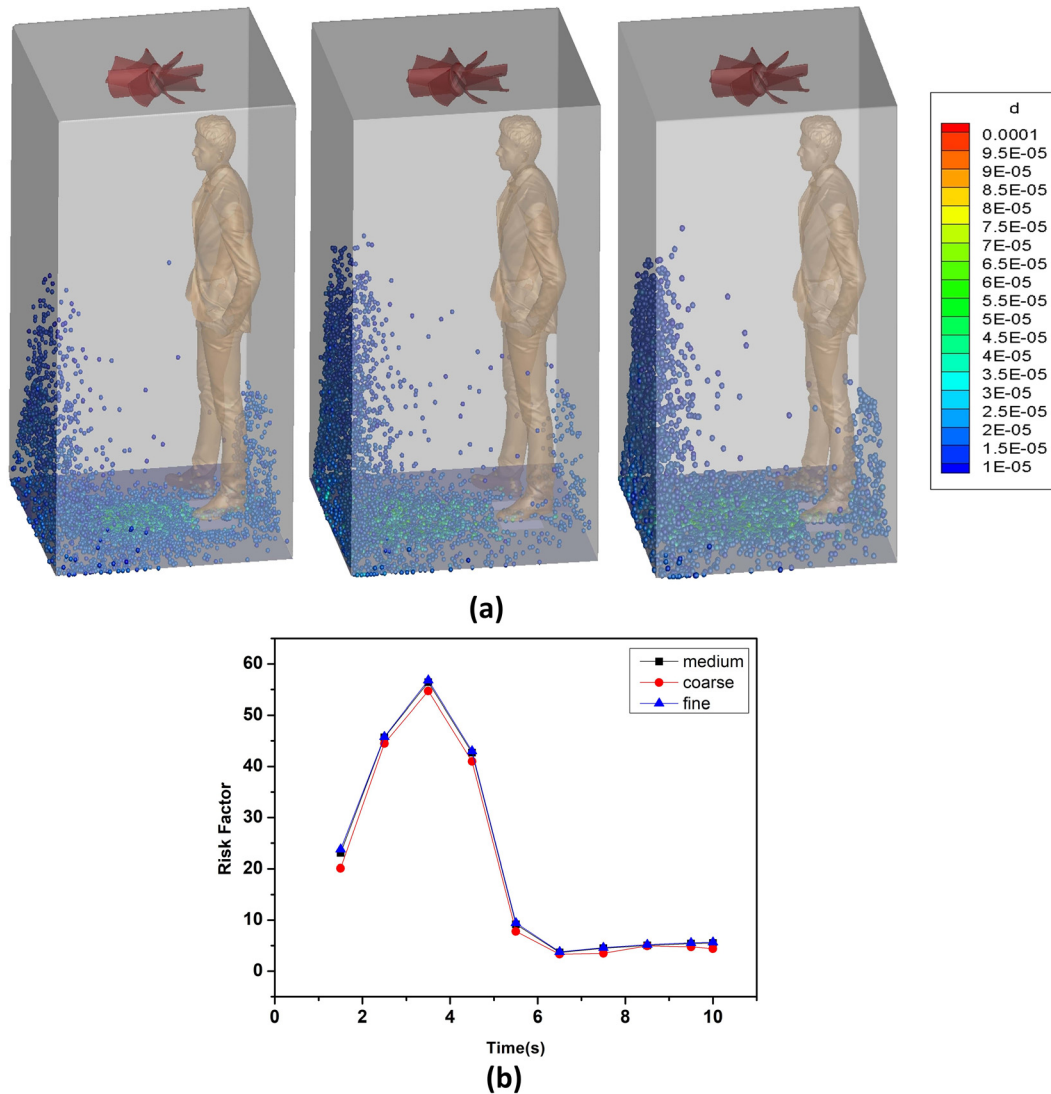


FIG. 20. (a) Comparisons of droplet distributions for coarse, medium, and fine mesh sizes, respectively, from left to right. (b) Comparisons of risk factors for coarse, medium, and fine mesh sizes, respectively, from left to right.

medium (578 669 cells), and fine (695 027 cells), have been considered. The normalized Eulerian field velocity V_y/V_{inlet} in a hot dry ambience having the top mounting implemented as an axial inlet jet ventilation condition ($V_{\text{inlet}} = 0.56 \text{ m/s}$) is taken as the parameter, against which the results of the three different meshes are compared in Fig. 21(b). The normalized axial velocity (V_y) profile is taken along a line AB of 0.6 m length, the line AB being parallel to the X axis. The line AB is situated on the plane CD. The plane CD is parallel to the elevator's floor and is at a height of 1 m above the elevator floor. The line AB and the plane CD and their positions inside the elevator domain are shown in Fig. 21(a). In addition to the normalized axial velocity (V_y) profile, the velocity magnitude contours on plane CD are also compared in Fig. 19(c). The droplet

dispersion and risk factors are compared in Figs. 20(a) and 20(b). From Figs. 19(b), 19(c), 20(a), and 20(b), it can be seen that the results of the coarse mesh vary considerably from that of the medium and fine mesh and that the results of the medium and fine mesh have negligible difference. Since the results become virtually grid independent with the medium and fine meshes, we adopted the medium mesh for our study. From this, it can be concluded that the medium mesh size considered here is adequate enough to capture the flow field correctly inside the elevator. Figures 21(a) and 21(b) show our finally adopted 3D mesh of 578 669 cells encapsulating the refinement near the boundaries and edges. Figure 21(c) shows a section of this mesh, which portrays the gradual refinement near the mouth.

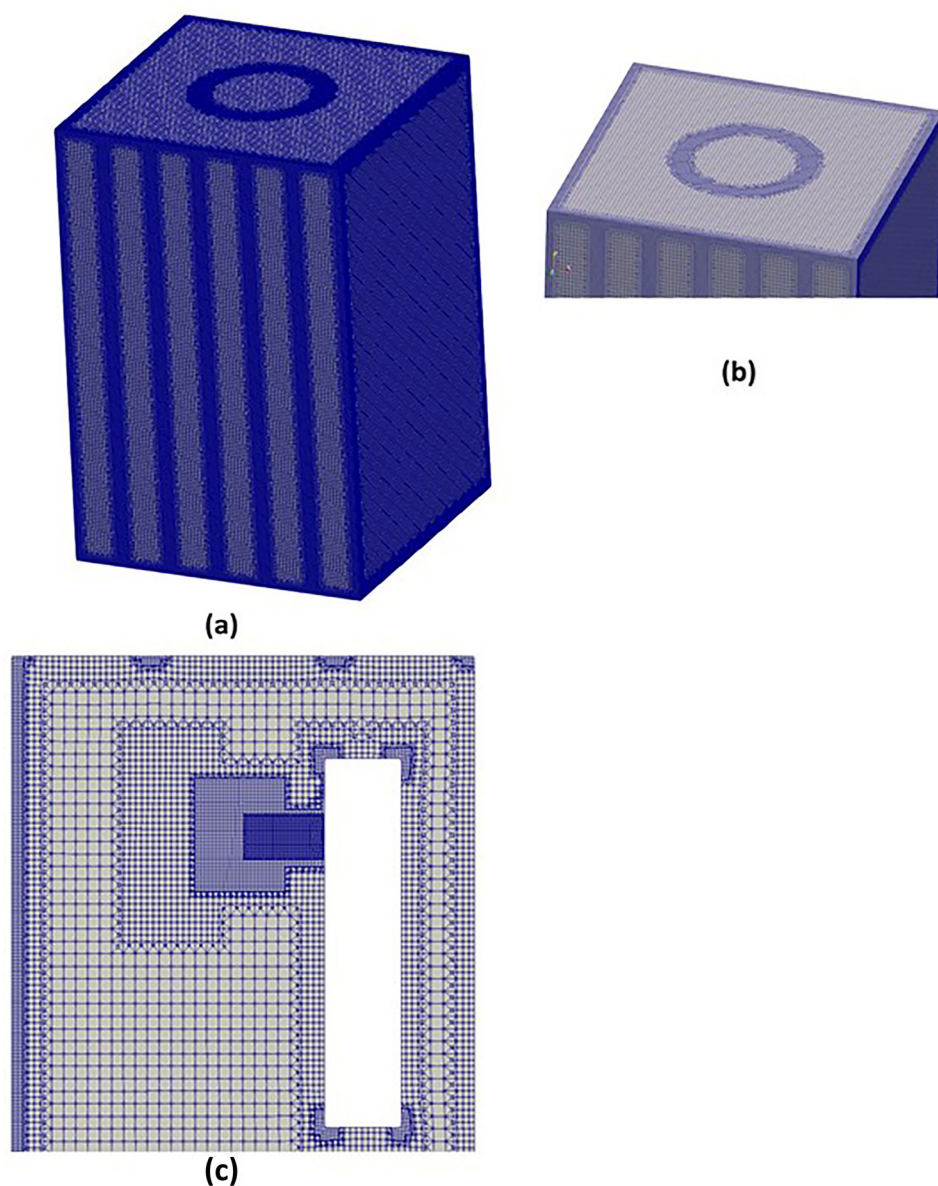


FIG. 21. (a) Adopted mesh, (b) refinements at various locations of the adopted mesh, and (c) mesh section showing gradual refinement of mesh near the mouth of the passenger.

REFERENCES

- ¹M. Richard, J. M. A. van den Brand, T. M. Bestebroer, P. Lexmond, D. de Meulder, R. A. M. Fouchier, A. C. Lowen, and S. Herfst, "Influenza A viruses are transmitted via the air from the nasal respiratory epithelium of ferrets," *Nat. Commun.* **11**(1), 766 (2020).
- ²World Health Organization, "CoronaTracker: World-wide COVID-19 outbreak data analysis and prediction," (Geneva World Heal. Organization, 2020), Vol. 19.
- ³L. Bourouiba, "The fluid dynamics of disease transmission," *Annu. Rev. Fluid Mech.* **53**, 473 (2021).
- ⁴L. Bourouiba, "Fluid dynamics of respiratory infectious diseases," *Annu. Rev. Biomed. Eng.* **23**, 547 (2021).
- ⁵L. Bourouiba, E. Dehandschoewercker, and J. W. M. Bush, "Violent expiratory events: On coughing and sneezing," *J. Fluid Mech.* **745**, 537 (2014).
- ⁶S. B. Kwon, J. Park, J. Jang, Y. Cho, D. S. Park, C. Kim, G. N. Bae, and A. Jang, "Study on the initial velocity distribution of exhaled air from coughing and speaking," *Chemosphere* **87**, 1260 (2012).
- ⁷G. R. Johnson, L. Morawska, Z. D. Ristovski, M. Hargreaves, K. Mengersen, C. Y. H. Chao, M. P. Wan, Y. Li, X. Xie, D. Katoshevski, and S. Corbett, "Modality of human expired aerosol size distributions," *J. Aerosol Sci.* **42**, 839 (2011).
- ⁸X. Li, Y. Shang, Y. Yan, L. Yang, and J. Tu, "Modelling of evaporation of cough droplets in inhomogeneous humidity fields using the multi-component Eulerian-Lagrangian approach," *Build. Environ.* **128**, 68 (2018).
- ⁹J. Redrow, S. Mao, I. Celik, J. A. Posada, and Z. gang Feng, "Modeling the evaporation and dispersion of airborne sputum droplets expelled from a human cough," *Build. Environ.* **46**, 2042 (2011).
- ¹⁰J. Wei and Y. Li, "Enhanced spread of expiratory droplets by turbulence in a cough jet," *Build. Environ.* **93**, 86 (2015).

- ¹¹R. Pal, S. Sarkar, and A. Mukhopadhyay, "Influence of ambient conditions on evaporation and transport of respiratory droplets in indoor environment," *Int. Commun. Heat Mass Transfer* **129**, 105750 (2021).
- ¹²K. L. Chong, C. S. Ng, N. Hori, R. Yang, R. Verzicco, and D. Lohse, "Extended lifetime of respiratory droplets in a turbulent vapor puff and its implications on airborne disease transmission," *Phys. Rev. Lett.* **126**, 034502 (2021).
- ¹³C. S. Ng, K. L. Chong, R. Yang, M. Li, R. Verzicco, and D. Lohse, "Growth of respiratory droplets in cold and humid air," *Phys. Rev. Fluids* **6**, 054303 (2021).
- ¹⁴H. Wang, Z. Li, X. Zhang, L. Zhu, Y. Liu, and S. Wang, "The motion of respiratory droplets produced by coughing," *Phys. Fluids* **32**(12), 125102 (2020).
- ¹⁵M. R. Pendar and J. C. Páscoa, "Numerical modeling of the distribution of virus evaporating saliva droplets during sneeze and cough," *Phys. Fluids* **32**, 083305 (2020).
- ¹⁶T. Dbouk and D. Drikakis, "On coughing and airborne droplet transmission to humans," *Phys. Fluids* **32**, 053310 (2020).
- ¹⁷Y. Feng, T. Marchal, T. Sperry, and H. Yi, "Influence of wind and relative humidity on the social distancing effectiveness to prevent COVID-19 airborne transmission: A numerical study," *J. Aerosol Sci.* **147**, 105585 (2020).
- ¹⁸H. Li, F. Y. Leong, G. Xu, Z. Ge, C. W. Kang, and K. H. Lim, "Dispersion of evaporating cough droplets in tropical outdoor environment," *Phys. Fluids* **32**, 113301 (2020).
- ¹⁹A. Foster and M. Kinzel, "Estimating COVID-19 exposure in a classroom setting: A comparison between mathematical and numerical models," *Phys. Fluids* **33**, 021904 (2021).
- ²⁰K. Talaat, M. Abuhegazy, and O. A. Mahfoze, "Simulation of aerosol transmission on a Boeing 737 airplane with intervention measures for COVID-19 mitigation," *Phys. Fluids* **33**, 033312 (2021).
- ²¹Y. Yan, X. Li, Y. Shang, and J. Tu, "Evaluation of airborne disease infection risks in an airliner cabin using the Lagrangian-based Wells-Riley approach," *Build. Environ.* **121**, 79 (2017).
- ²²H. Liu, S. He, L. Shen, and J. Hong, "Simulation-based study of COVID-19 outbreak associated with air-conditioning in a restaurant," *Phys. Fluids* **33**, 023301 (2021).
- ²³L. Wu, X. Liu, F. Yao, and Y. Chen, "Numerical study of virus transmission through droplets from sneezing in a cafeteria," *Phys. Fluids* **33**, 023311 (2021).
- ²⁴X. Yang, C. Ou, H. Yang, L. Liu *et al.*, "Transmission of pathogen-laden expiratory droplets in a coach bus," *J. Hazard. Mater.* **397**, 122609 (2020).
- ²⁵J. Komperda, A. Peyvan, D. Li, B. Kashir, A. L. Yarin, C. M. Megaridis, P. Mirbod, I. Paprotny, L. F. Cooper, S. Rowan, C. Stanford, and F. Mashayek, "Computer simulation of the SARS-CoV-2 contamination risk in a large dental clinic," *Phys. Fluids* **33**, 033328 (2021).
- ²⁶F. Liu, H. Qian, Z. Luo, S. Wang, and X. Zheng, "A laboratory study of the expiratory airflow and particle dispersion in the stratified indoor environment," *Build. Environ.* **180**, 106988 (2020).
- ²⁷C. H. Cheng, C. L. Chow, and W. K. Chow, "Trajectories of large respiratory droplets in indoor environment: A simplified approach," *Build. Environ.* **183**, 107196 (2020).
- ²⁸Y. Yan, X. Li, and J. Tu, "Thermal effect of human body on cough droplets evaporation and dispersion in an enclosed space," *Build. Environ.* **148**, 96 (2019).
- ²⁹N. Sen, "Transmission and evaporation of cough droplets in an elevator: Numerical simulations of some possible scenarios," *Phys. Fluids* **33**(3), 033311 (2021).
- ³⁰T. Dbouk and D. Drikakis, "On airborne virus transmission in elevators and confined spaces," *Phys. Fluids* **33**, 011905 (2021).
- ³¹A. Agrawal and R. Bhardwaj, "Tailoring surface wettability to reduce chances of infection of COVID-19 by a respiratory droplet and to improve the effectiveness of personal protection equipment," *Phys. Fluids* **32**, 081702 (2020).
- ³²M. Jayaweera, H. Perera, B. Gunawardana, and J. Manatunge, "Transmission of COVID-19 virus by droplets and aerosols: A critical review on the unresolved dichotomy," *Environ. Res.* **188**, 109819 (2020).
- ³³T. Dbouk and D. Drikakis, "On respiratory droplets and face masks," *Phys. Fluids* **32**(6), 063303 (2020).
- ³⁴S. H. Smith, G. A. Somsen, C. van Rijn, S. Kooij, L. van der Hoek, R. A. Bem, and D. Bonn, "Aerosol persistence in relation to possible transmission of SARS-CoV-2," *Phys. Fluids* **32**, 107108 (2020).
- ³⁵K. Ashwini, A. K. Anjali, and V. Sivaswamy, "Role of aerosols in the spread of COVID-19-A review," *Int. J. Res. Pharm. Sci.* **11**, 1022 (2020).
- ³⁶T. Greenhalgh, J. L. Jimenez, K. A. Prather, Z. Tufekci, D. Fisman, and R. Schooley, "Ten scientific reasons in support of airborne transmission of SARS-CoV-2," *Lancet* **397**, 1603 (2021).
- ³⁷J. Akhtar, A. L. Garcia, L. Saenz, S. Kuravi, F. Shu, and K. Kota, "Can face masks offer protection from airborne sneeze and cough droplets in close-up, face-to-face human interactions?-A quantitative study," *Phys. Fluids* **32**, 127112 (2020).
- ³⁸"Safety rules for the construction and installation of lifts - Part 1: Electric lifts," Standard No. EN 81-1:1998 (Central Secretariat: Rue de Stassart, 1998).
- ³⁹S. A. Chillon, A. Ugarte-Anero, I. Aramendia, U. Fernandez-Gamiz, and E. Zulueta, "Numerical modeling of the spread of cough saliva droplets in a calm confined space," *Mathematics* **9**(5), 574 (2021).
- ⁴⁰H. Jasak, "OpenFOAM: Open source CFD in research and industry," *Int. J. Nav. Archit. Ocean Eng.* **1**, 89–94 (2009).
- ⁴¹F. R. Menter, "Two-equation eddy-viscosity turbulence models for engineering applications," *AIAA J.* **32**, 1598–1605 (1994).
- ⁴²W. E. Ranz and W. R. Marshall, "Evaporation from drops. Part I," *Chem. Eng. Prog.* **48**, 141–146 (1952).
- ⁴³W. E. Ranz and W. R. Marshall, "Evaporation from drops. Part II," *Chem. Eng. Prog.* **48**, 173–180 (1952).
- ⁴⁴S. Basu, P. Kabi, S. Chaudhuri, and A. Saha, "Insights on drying and precipitation dynamics of respiratory droplets from the perspective of COVID-19," *Phys. Fluids* **32**(12), 123317 (2020).
- ⁴⁵W. Sutherland, "The viscosity of gases and molecular force," *Philos. Mag.* **36**, 507–531 (1893).
- ⁴⁶"National Building Code of India—Bureau of Indian Standards," Manak Bhavan, 9 Bahadur Shah Zafar Marg, New Delhi, 110 002 (Sunshine Process, C-105/5, Naraina Industrial Area, Phase 1, 2005).
- ⁴⁷American Society of Mechanical Engineers, "Safety code for elevators and escalators" (American Society of Mechanical Engineers, New York, 2010) Standard No. ASME A17.1-2010.
- ⁴⁸C. E. Junge, *Air Chemistry and Radioactivity*, International Geophysics Series (Academic Press, 1963), Vol. 4.
- ⁴⁹A. F. Miguel, "Penetration of inhaled aerosols in the bronchial tree," *Med. Eng. Phys.* **44**, 25–31 (2017).